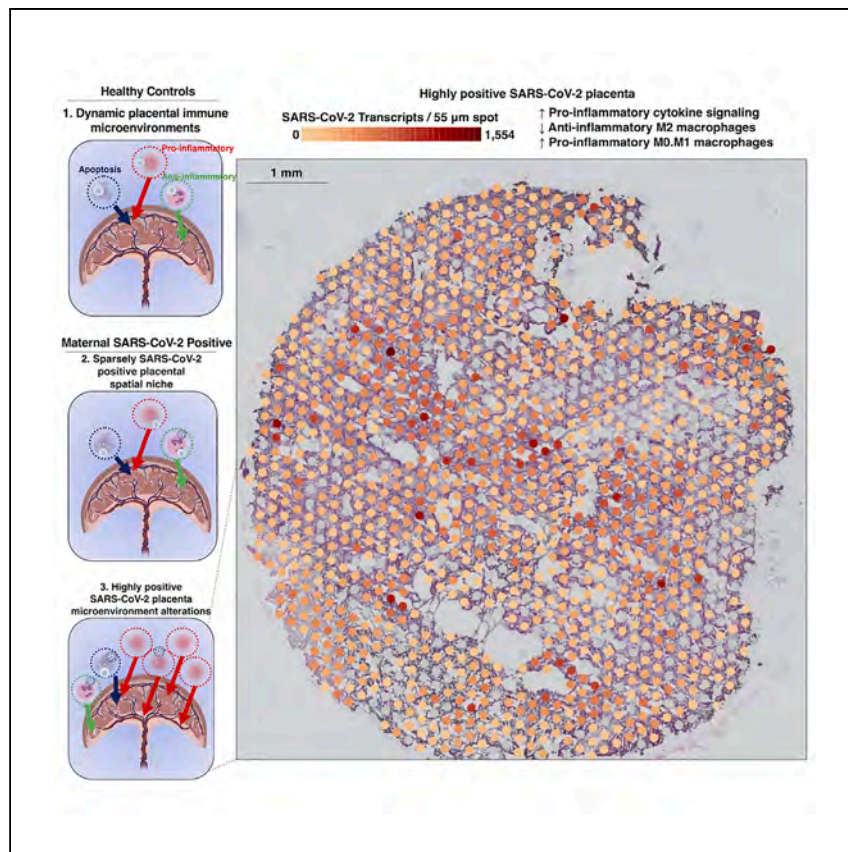# Med

Clinical and Translational Article

SARS-CoV-2 niches in human placenta revealed by spatial transcriptomics

Barrozo et al. map gene expression in term placental microenvironments with orthogonal bulk and spatial approaches to parse how functional placental niches restrict vertical transmission of pathogens. Applying this atlas to cases of maternal SARS-CoV-2 infections revealed divergent placental immune microenvironments associated with asymptomatic infection and clinically evident disease.

Translation to Patients

Enrico R. Barrozo, Maxim D. Seferovic, Eumenia C.C. Castro, ..., Ricardo Ferral Rojas, Cynthia D. Shope, Kjersti M. Aagaard

aagaardt@bcm.edu

Highlights

Term placenta transcriptomics atlas with spatial and single-cell resolution

Transcriptomic niches of sparse or high SARS-CoV-2 levels in placentae

SARS-CoV-2 infection may lead to a range of dynamic placental immune microenvironments

Clinical and Translational Article

SARS-CoV-2 niches in human placenta revealed by spatial transcriptomics

Enrico R. Barrozo,[1] Maxim D. Seferovic,[1] Eumenia C.C. Castro,[2] Angela M. Major,[2]
David N. Moorshead,[1,3,4] Michael D. Jochum,[1] Ricardo Ferral Rojas,[1] Cynthia D. Shope,[1]
and Kjersti M. Aagaard[1,5,*]

SUMMARY

Background: Functional placental niches are presumed to spatially separate maternal-fetal antigens and restrict the vertical transmission of pathogens. We hypothesized a high-resolution map of placental transcription could provide direct evidence for niche microenvironments with unique functions and transcription profiles.

Methods: We utilized Visium Spatial Transcriptomics paired with H&E staining to generate 17,927 spatial transcriptomes. By integrating these spatial transcriptomes with 273,944 placental single-cell and single-nuclei transcriptomes, we generated an atlas composed of at least 22 subpopulations in the maternal decidua, fetal chorionic villi, and chorioamniotic membranes.

Findings: Comparisons of placentae from uninfected healthy controls (n = 4) with COVID-19 asymptomatic (n = 4) and symptomatic (n = 5) infected participants demonstrated that severe acute respiratory syndrome coronavirus 2 (SARS-CoV-2) detection in syncytiotrophoblasts occurred in both the presence and the absence of maternal clinical disease. With spatial transcriptomics, we found that the limit of detection for SARS-CoV-2 was 1/7,000 cells, and placental niches without detectable viral transcripts were unperturbed. In contrast, niches with high SARS-CoV-2 transcript levels were associated with significant upregulation in pro-inflammatory cytokines and interferon-stimulated genes, altered metallopeptidase signaling (*TIMP1*), with coordinated shifts in macrophage polarization, histiocytic intervillositis, and perivillous fibrin deposition. Fetal sex differences in gene expression responses to SARS-CoV-2 were limited, with confirmed mapping limited to the maternal decidua in males.

Conclusions: High-resolution placental transcriptomics with spatial resolution revealed dynamic responses to SARS-CoV-2 in coordinate microenvironments in the absence and presence of clinically evident disease.

Funding: This work was supported by the NIH (R01HD091731 and T32-HD098069), NSF (2208903), the Burroughs Welcome Fund and the March of Dimes Preterm Birth Research Initiatives, and a Career Development Award from the American Society of Gene and Cell Therapy.

INTRODUCTION

Not all gravidae (pregnant persons) infected with severe acute respiratory syndrome coronavirus 2 (SARS-CoV-2) will experience symptoms or suffer COVID-19.[1–6] However, we and others have provided key data demonstrating a disproportionate risk of

CONTEXT AND SIGNIFICANCE

With placentae collected during the SARS-CoV-2 Delta variant surge, when the burden of COVID-19 on maternal-fetal health was at its peak, researchers at Baylor College of Medicine utilized state-of-the-art approaches to characterize distinct functional roles in the maternal and fetal spaces of the placenta and showed differences ranging from healthy uninfected to highly SARS-CoV-2-infected areas with clinically evident disease. These data suggest that multiple mechanisms lead to the clearance of sparse SARS-CoV-2 placental infections and identify potential SARS-CoV-2-susceptible areas or "niches" that persist up to 10 days after the onset and resolution of symptoms.

COVID-19 mortality and morbidity during pregnancy with a greater burden among vulnerable populations.[7–15] In seeking to understand this disproportionate risk burden during pregnancy, several studies have sought to examine associations between maternal COVID-19, placental immunity, SARS-CoV-2 intraamniotic infection, and fetal disease.[11,16–22] Using mid- to low-resolution approaches, the available literature suggests that although SARS-CoV-2 can enter and replicate in placental trophoblast cells, maternal-fetal vertical transmission *in utero* rarely occurs (<1%), and there is no clear association between SARS-CoV-2 replication in the placenta and gross histopathology.[10,11,17,19,20,23–26] Single-cell RNA sequencing (RNA-seq; scRNA-seq) atlases offer a higher-resolution approach aimed at providing molecular insight into the pathogenesis of COVID-19, with the identification of cells expressing viral receptors and entry co-factors, descriptions of rare subtypes of cells associated with increased disease severity, and the identification of distinct cytokine storm transcription programs.[27–33] Of interest to our work herein, initial placental bulk RNA-seq and scRNA-seq analyses of SARS-CoV-2 entry receptor *ACE2* and co-factor *TMPRSS2* yielded conflicting results on whether SARS-CoV-2 could enter or replicate in placental cells,[34–37] the degree of inflammatory signaling, macrophage and T cell recruitment, and susceptibility varying by sex.[19,21,38–43] Prior studies did not detect SARS-CoV-2 transcripts within the placenta single-cell transcriptomes, limiting insight into the host responses to SARS-CoV-2 within the placenta.

In the current study, we sought to overcome prior limitations by pairing bulk assays, microscopy, and 10× Genomics Visium Spatial Transcriptomics (v2) to create a high-resolution map of normal placental spatial niches and to compare uninfected controls with placentae from both symptomatic and asymptomatic maternal SARS-CoV-2-positive (mSARS-CoV-2+) cases (as defined by positive nasopharyngeal swabs within 72 h of delivery). We hypothesized that a high-resolution single-cell and spatial placental transcriptomics atlas would reveal molecular mechanisms of normal placental immune tolerance and detect immune activation in microenvironments permissive to efficient SARS-CoV-2 replication. We generated placental spatial transcriptomes in placentae from healthy SARS-CoV-2− participants (n = 4) and compared them with placentae from SARS-CoV-2+ gravidae (n = 9). Maternal subjects positive for SARS-CoV-2 were either asymptomatic (no COVID-19-related symptoms, n = 4) or symptomatic (cough, fever, pneumonia, and/or respiratory failure, n = 5). We employed rigorous orthogonal methods, including immunohistochemistry (IHC), RNA *in situ* hybridization (RNAscope), bulk RT-qPCR, and spatial transcriptomics, to assess the limits of detection for SARS-CoV-2 in placentae. We found that SARS-CoV-2 detection in the placenta by RT-qPCR or spatial transcriptomics was just as likely in asymptomatic participants (three of four cases) as those with symptomatic maternal COVID-19 (four of five cases). Specifically, we found no SARS-CoV-2 in three placentae from known infected gravidae, five cases of sparse SARS-CoV-2 placental transcripts, and two placentae from term and preterm intrauterine fetal demise (IUFD) cases highly positive for SARS-CoV-2 transcripts. With these placentae, we profiled the distinct host and SARS-CoV-2 changes in transcript levels with a high degree of spatial resolution, and we used these data to propose a comprehensive model representative of distinct phases of probable SARS-CoV-2 infection at the maternal-fetal interface.

RESULTS

Participant cohorts and their clinical characteristics
We and other have previously used high-resolution molecular approaches to visualize bacteria and viruses in placental tissue in the absence of overt histopathology

[1]Department of Obstetrics and Gynecology, Division of Maternal-Fetal Medicine, Baylor College of Medicine and Texas Children's Hospital, Houston, TX, USA

[2]Department of Pathology and Immunology, Baylor College of Medicine and Texas Children's Hospital, Houston, TX, USA

[3]Medical Scientist Training Program, Baylor College of Medicine, Houston, TX, USA

[4]Immunology and Microbiology Graduate Program, Baylor College of Medicine, Houston, TX, USA

[5]Lead contact

*Correspondence: aagaardt@bcm.edu

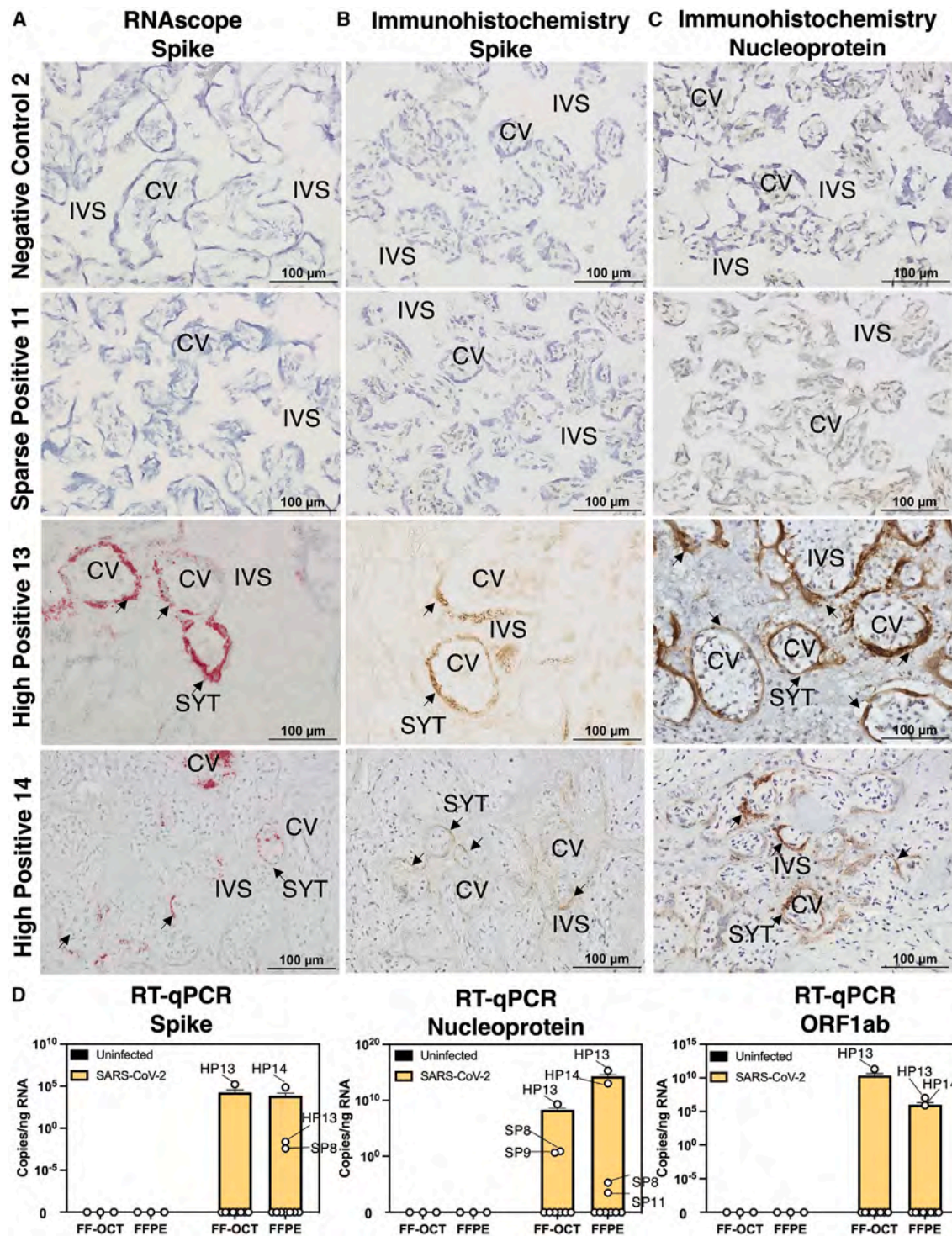https://doi.org/10.1016/j.medj.2023.06.003

Figure 1. Detection of SARS-CoV-2 in placentae by histology and bulk RT-qPCR

(A–C) Fresh-frozen in optimal cutting temperature serum (FF-OCT) tissue blocks from spatial transcriptomics samples were cryosectioned and subject to (A) RNA *in situ* probing for SARS-CoV-2 Spike (S), (B) immunohistochemistry (IHC) for S, and (C) IHC staining for SARS-CoV-2 Nucleocapsid (N). Images were taken at 20× magnification, and each row represents images obtained from an individual participant.

(D) FF-OCT and formalin-fixed and paraffin-embedded (FFPE) blocks were subject to RT-qPCR probing for S, N, or ORF1ab SARS-CoV-2 transcripts. Based on these results, placentae were grouped for analysis into negative controls (NCs), maternal positive but SARS-CoV-2 was not detected in the placenta (ND), sparse positive (SP) if SARS-CoV-2 was detected by RT-qPCR where ct values <27 were observed (limit of detection = 1/7,000 cells) or ≥1

Figure 1. Continued

SARS-CoV-2 transcripts per spot were observed spatial transcriptomics (limit of detection = 1/661 cells), and high positive (HP) where RT-qPCR ct values < 15 and ≥2–1,554 SARS-CoV-2 transcripts per spot were observed. Error bars represent the standard error of the mean.

CV, chorionic villi; IVS, intervillous space; SYT, syncytiotrophoblast.

and inflammation.[20,44–59] Therefore, we used these and other recently developed high-resolution technologies (including the Visium 10× platform) in a set of orthogonal methods to profile placental immune microenvironments with or without mSARS-CoV-2 infection. The 14 placentae were given unique identifiers (1–14) and grouped by maternal infection and disease status for comparative analysis. Analysis cohorts included negative controls (NCs; n = 4) and mSARS-CoV-2+ participants (n = 10). In the latter category, although all mSARS-CoV-2+ participants had tested positive by clinical nasopharyngeal swab within 72 h of delivery (see Table S1, ST1.1, and Table S2), not all participants had detectable viral transcripts in the placenta. We therefore designated the mSARS-CoV-2+ participants as not detected in the placenta (ND), sparse positive (SP) if SARS-CoV-2 was detected by RT-qPCR ct values < 27 for SARS-CoV-2 transcripts (limit of detection = 1/7,000 cells) or ≥1 SARS-CoV-2 transcripts/spot by spatial transcriptomics (limit of detection = 1/661 cells), or high-positive (HP) placentae where RT-qPCR ct values < 15 were observed for SARS-CoV-2 transcripts or ≥2–1,554 SARS-CoV-2 transcripts/spot by spatial transcriptomics. We did not detect a false-positive alignment to a SARS-CoV-2 transcript with our >5.8 billion spatial transcriptomics data and independent alignment of published[19,34,60–62] scRNA-seq reads.

The clinical characteristics of this study's cohorts are summarized in Table S2, and subject metadata are available in Table S1, ST1.1. mSARS-CoV-2 placentae and uninfected controls were collected between August and October 2021 during the Delta (B.1.617.2) variant surge.[63,64] None of the subjects had received SARS-CoV-2 vaccine doses before or during pregnancy, and none of the offspring tested positive for SARS-CoV-2 after delivery. Placentae from uninfected NCs (n = 4 subjects) included one female placenta with a female fetus sampled from the chorionic villi, decidua, and chorioamniotic membranes (NC1a, NC1b, and NC1c), and three placentae from male fetuses were each sampled once from the parenchyma (NC2, NC3, and NC4). Sampling pre-defined regions allowed us to compare uniform parenchymal sections in an unbiased manner. We collected placentae from mSARS-CoV-2+ participants who were asymptomatic (n = 4 subjects: two male and two female fetuses), and we also collected placentae from mSARS-CoV-2+ subjects exhibiting COVID-19 symptoms, including pneumonia and maternal respiratory failure (n = 6 subjects: two male, three female, and one not disclosed fetus). Among symptomatic gravidae, the most common diagnosis was SARS-CoV-2 pneumonia (*p < 0.05), and the onset of symptoms averaged 7 days before delivery (*p < 0.05). Of note, placenta sample HP13 was a preterm (22.3 weeks' gestation) IUFD case highly positive for SARS-CoV-2 and was sampled twice for spatial transcriptomics, whereas HP14 was a case of IUFD (35 weeks' gestation) where fresh tissue was not available for the Visium Spatial Transcriptomics platform.

Detection of placental SARS-CoV-2 employing orthogonal methods

First, we performed microscopy including RNA *in situ* hybridization (RNAscope) to localize SARS-CoV-2 spike transcripts and stained for viral proteins spike and nucleoprotein with IHC (Figure 1; see summary of all microscopy results for each sample in Table S1, ST1.1). We did not observe spike RNA, spike protein, or nucleoprotein microscopically in any mSARS-CoV-2 NC, nor in all samples with a positive maternal RT-qPCR nasal swab (mSARS-CoV-2+, ND). Using our NCs and serial dilutions of a

SARS-CoV-2 cDNA template, we determined the limit of detection for SARS-CoV-2 spike, nucleoprotein, and ORF1ab by one-step RT-qPCR to be one copy of viral RNA per 3,000 cells. The ct values and absolute quantities of SARS-CoV-2 transcripts are available in Table S1, ST1.1. We performed RT-qPCR from fresh-frozen samples preserved in optimal cutting temperature solution (FF-OCT) and formalin-fixed paraffin-embedded (FFPE) samples from the same placentae. We found high SARS-CoV-2 spike, nucleoprotein, and ORF1ab in HP13 (ct 11–34) and HP14 (ct 18–22). In addition, we observed sparse levels (ct 26–39) of SARS-CoV-2 transcripts in three additional samples (SP8, SP9, and SP11). Based on the consensus standardized NIH-NICHD (Eunice Kennedy Shriver National Institute of Child Health and Human Development) definition of placental SARS-CoV-2,[65] cases HP13 and HP14 meet the criteria for probable replication based on the detection of both viral protein and vRNA. Therefore, we infer SARS-CoV-2 replication in these cases but cannot confirm or deny replication in the sparsely positive cases.

Generation of a term placenta transcriptomics atlas with spatial and single-cell resolution

We utilized the 10× Genomics Visium spatial transcriptomics platform for fresh tissue, which captures polyadenylated RNAs, including SARS-CoV-2, but currently does not yield single-cell resolution (55-μm spots that capture RNA from one to five cells). Therefore, we also analyzed published placental scRNA-seq or single-nuclei RNA-seq (snRNA-seq) datasets[19,34,60–62] to generate an inclusive placenta cell-type transcriptome reference. We independently analyzed 273,944 placenta single-cell and single-nuclei transcriptomes, annotated each cluster with a cell type based on canonical marker gene expression (Log_2(fold-change) > 2, Wilcoxon rank-sum test adjusted p < 0.05), and integrated these data with our newly generated placenta spatial transcriptomics data using anchoring features shared among platforms (Figure 2; atlas differential expression results available in Table S1, ST1.2). We found overlap between the spatial and snRNA-seq datasets but relatively poor overlap with the scRNA-seq data, potentially because of known technical biases between Visium (v2), snRNA-seq, and scRNA-seq approaches, which may or may not exclude large multi-nucleated syncytiotrophoblasts (SYTs) that comprise the maternal-fetal barrier.[66] Anchor-based integration and probabilistic transfer of single-cell annotations have been utilized to determine near-single-cell niches from spatial transcriptomics data.[67] Therefore, we used the annotations of the term single-cell atlas to assess the predictiveness of each spatial transcriptome cluster aligning with single-cell niches. We found high conservation between spatial and single-cell profiles of placental cell types, including SYT and extravillous trophoblasts (EVTs), and we also identified spatial transcriptome spots aligning with the single-cell transcriptomic profiles of macrophages (Figure 2B).

After stringent quality-control filtering (Figure S1A), 17,927 spatial transcriptomes from 16 samples were visualized in two-dimensional Unique Manifold Approximation and Projection (UMAP) space (Figure 2C). Clustering resulted in 22 subpopulations, which were annotated based on the prediction values from the reference single-cell term placenta atlas and significant upregulation (Log_2(fold-change) > 2, q < 0.05) of marker transcripts. For example, transcription niches predicted as stromal cells were marked by significant upregulation of *IGFBP1* and *PRL* expression. Notably, there were no significant differences in the proportions of spatial transcriptomes among samples (Table S1, ST1.3). None of the clusters were defined by batch effects or quality-control metrics, including cell-cycle gene expression, the number of unique genes per spot, the number of unique molecule identifiers (UMIs) per spot, mitochondrial gene expression, or ribosomal genes (Figure S1). The spatial
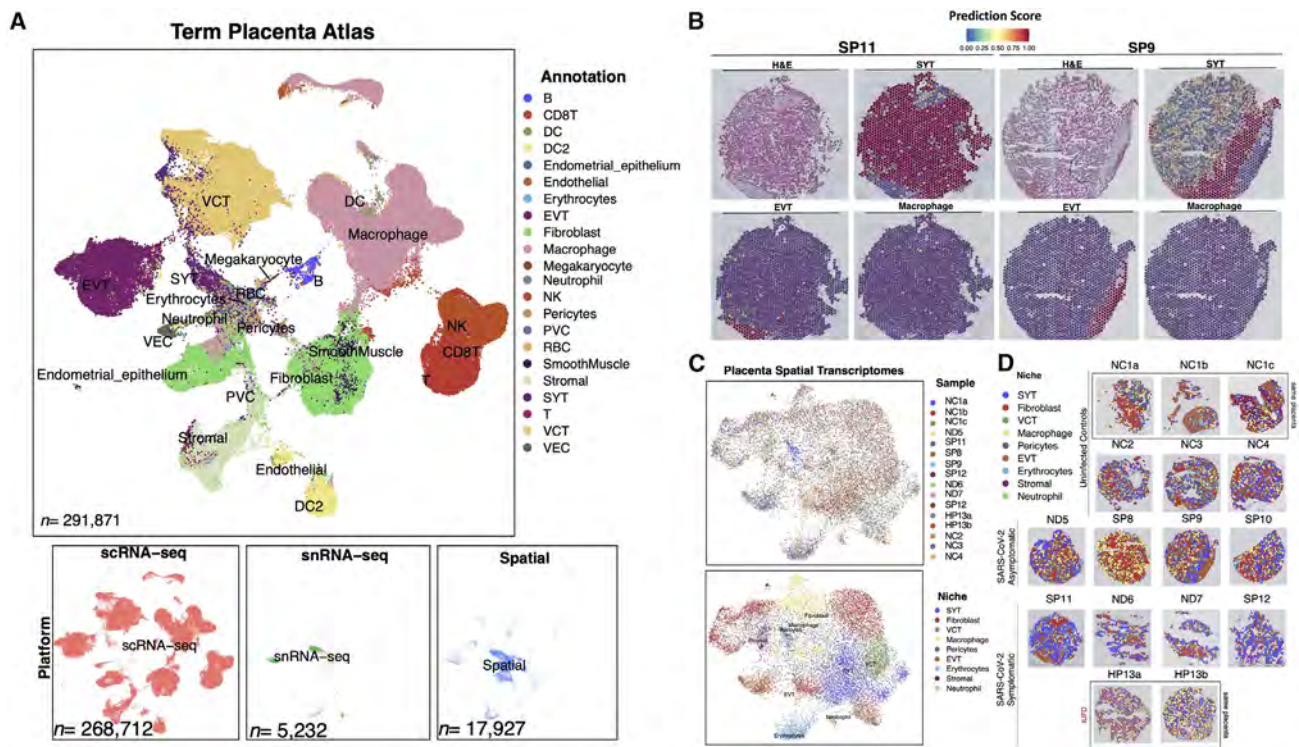
Figure 2. A term single-cell and spatial transcriptomics atlas predicts cell-type niches with or without SARS-CoV-2

(A and B) (A) With 273,944 placenta single-cell and single-nuclei transcriptomes, a term placenta single-cell transcriptomics atlas was generated and used to (B) predict the cell-type profiles of the spatial transcriptomics niches.

(C) Dimension reduction Unique Manifold Approximation and Projection (UMAP) of the 17,927 spatial transcriptomics labeled by analysis cohort or niche annotation.

(D) Spatial locations of each transcriptomics niche for each sample.

DC, dendritic cell; EVT, extravillous trophoblast; NK, natural killer cell; PVC, perivillous cell; RBC, red blood cell; VCT, villous cytotrophoblast; VEC, vascular endothelial cell.

transcriptome niche annotations were overlaid on top of the H&E images for each sample (Figure 2D), aligning with pathologist-annotated structural and histopathology features and permitting the discovery of distinct microenvironments. The expert placenta pathologist annotations and high-resolution H&E images are available for interactive analysis with the Loupe Cell Browser software (available for download at https://osf.io/mbfuv/?view_only=892cd90b5eb04e42bdbc18e04a102336).

Transcriptomic niches of sparse or high SARS-CoV-2 levels in placentae

Next, we aimed to determine which placental spatial transcriptomics niches allowed for the detection of SARS-CoV-2, and we assessed the limits of detection for SARS-CoV-2 using Visium. The false-positive rate aligning SARS-CoV-2$^-$ transcriptomes to the human and SARS-CoV-2 reference was low (0 out of >300 million spatial transcriptomics reads and 0 out of 5 billion scRNA-seq and snRNA-seq reads). No SARS-CoV-2 transcripts were detected in the placentae of four healthy NCs, one placenta from asymptomatic mSARS-CoV-2$^+$ cases, and two placentae from symptomatic mSARS-CoV-2$^+$ cases. In spatial transcriptomes, we observed SARS-CoV-2 transcripts ranging from as sparse as 1 SARS-CoV-2 transcript detected in a sample to levels as high as 1,554 viral transcripts (Figure 3; spatial expression of all SARS-CoV-2 genes is visualized in Figure S2). From symptomatic mSARS-CoV-2$^+$ subjects, three of the five placentae were positive for SARS-CoV-2 in the spatial datasets. There were 752 spatial transcriptomes with viral transcripts (raw counts in
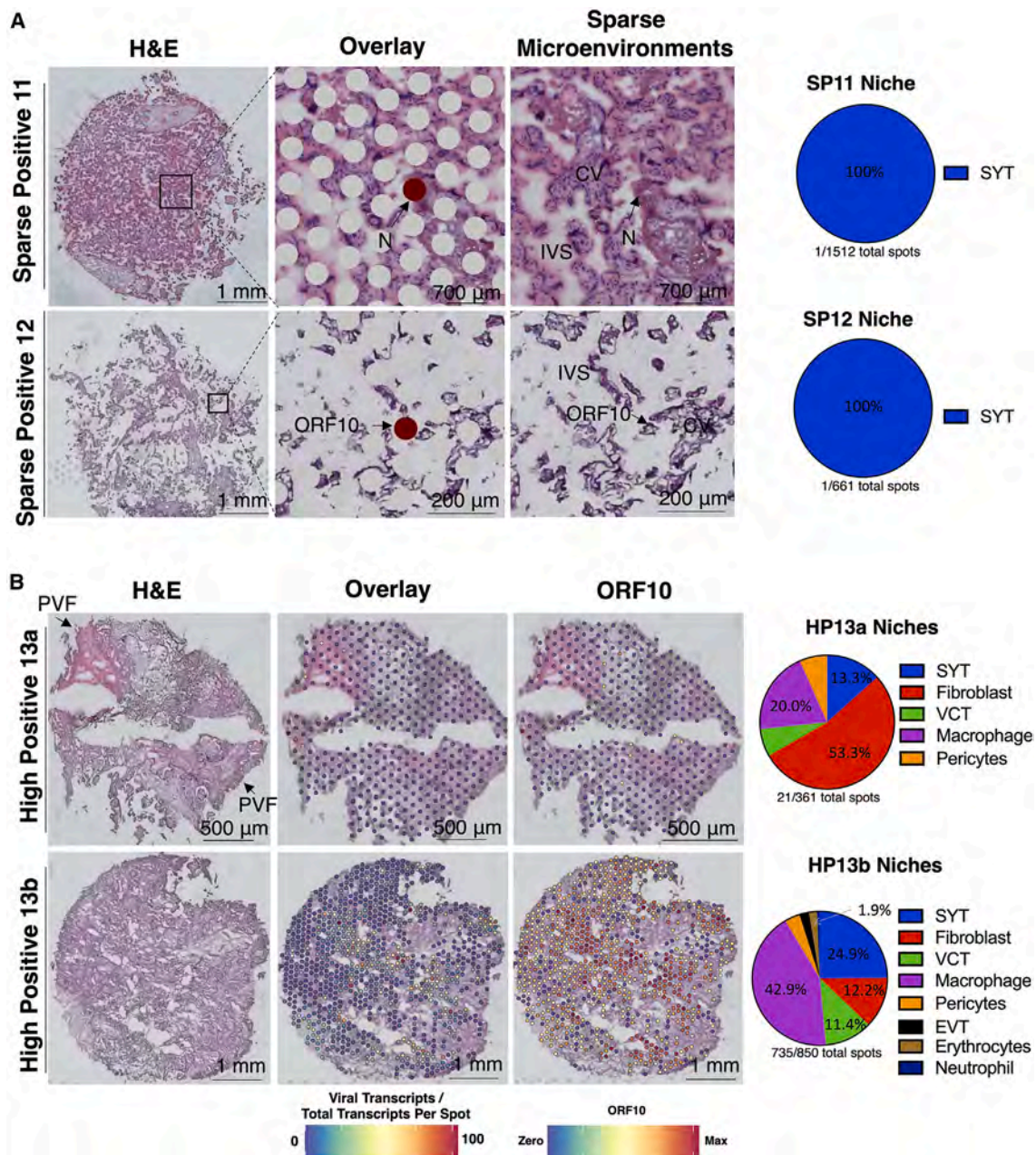
Figure 3. Transcriptomic niches of sparse or high SARS-CoV-2 levels in placentae

(A) H&E stain of sparsely positive SARS-CoV-2 placentae with the H&E, spatial transcriptome overlay, and zooming in on areas of SARS-CoV-2 transcript detection. The pie charts reveal how many spatial transcriptome spots were positive for SARS-CoV-2 and the annotation of those spots. The IVS and CV are labeled. Each row represents images from a separate participant. The niches in the pie charts refer to the spatial transcriptome annotation.

(B) H&E stain of highly positive SARS-CoV-2 placenta samples annotating areas with perivillous fibrinoid (PVF) deposition or SARS-CoV-2 transcripts. Each row represents images in separate sections from participant HP13.

Table S1, ST1.1 and ST1.5). We found our limit of detection for SARS-CoV-2 in placental spatial transcriptomics data was 1 in approximately 700 cells, resembling that of RT-qPCR. There was one N transcript in an SYT niche for SP11 and one ORF10 transcript in an SYT niche for SP12 (Figure 3A). Although HP13 and HP13b were sampled from the same placenta, HP13b had 735 spots with 14,213 SARS-CoV-2 transcripts, including all SARS-CoV-2 RNAs. In comparison, HP13a had 15 spots
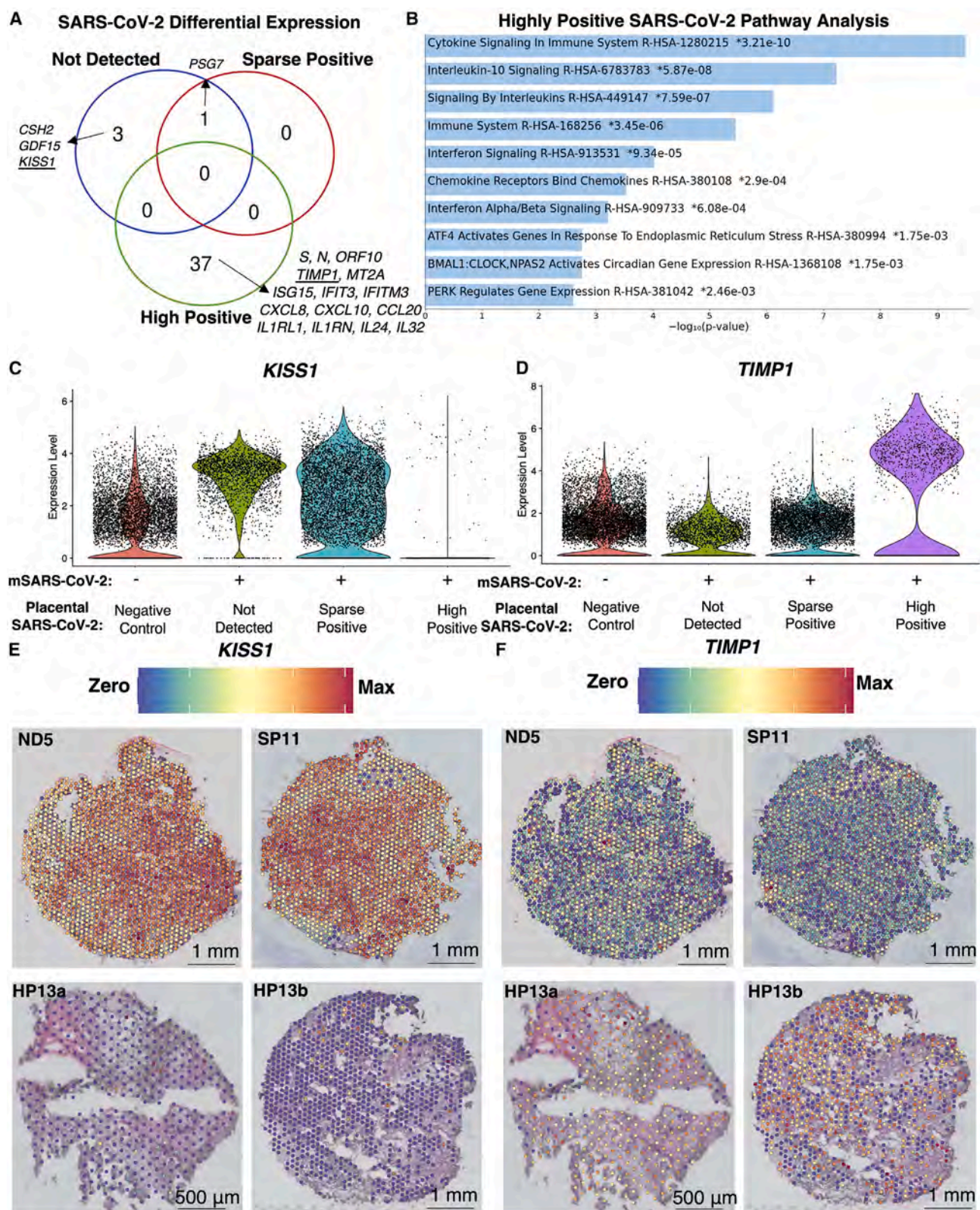
A SARS-CoV-2 Differential Expression

B Highly Positive SARS-CoV-2 Pathway Analysis

C *KISS1*

D *TIMP1*

E *KISS1*

F *TIMP1*

Figure 4. Unique spatial transcription markers in placentae depending on SARS-CoV-2 detection levels

(A) Differential expression between spatial transcriptomes in each analysis cohort relative to the NCs identified 54 significantly differentially expressed transcripts ($q < 0.05$, Log$_2$(fold-change) > 2) unique or shared between analysis cohorts.

(B) The 37 transcripts unique to highly positive SARS-CoV-2 placentae were subject to EnrichR pathway analysis with the Reactome 2022 database, revealing the top 90th quartile of significant ($q < 0.05$) pathways.

(C and D) Violin plots with the expression levels of *KISS1* and *TIMP1*, which were markers for placentae where SARS-CoV-2 was not detected or highly positive, respectively.

(E and F) Spatial gene expression of *KISS1* and *TIMP1* representative of each analysis cohort.

with SARS-CoV-2 transcripts, including 3 ORF1ab, 1 N, and 17 ORF10 counts ranging from 1 to 4 viral transcripts per spot in SYT, fibroblast, villous cytotrophoblast (VCT), macrophage, and pericyte niches. The pie charts niches reflect 55-μm microenvironments composed of one to five cells captured by spatial transcriptomics that were annotated utilizing the single-cell and single-nuclei references and do not imply viral replication within these cell types. The SARS-CoV-2 ORF10 transcript was the most abundant, making up approximately 86% of viral transcripts. However, this could be because of technical bias because reverse transcription was initiated by a poly(dT) primer. SARS-CoV-2 transcripts were detected in all spatial transcriptomics niches except for stromal. There were 14 spots with viral transcripts predicted to be erythrocytes based on hemoglobin expression, potentially representing maternal blood. Interestingly, most (42%) of the SARS-CoV-2 transcripts in HP13b were observed in macrophage niches. Because perivillous fibrin deposition was observed in the HP13a section, but not in HP13b, HP13a could be at the end stages of inflammation exhibiting necrosis, whereas HP13b could be in the earlier stages of inflammation with high amounts of SARS-CoV-2 RNA.

Unique spatial transcription markers in placentae associated with a range of SARS-CoV-2 detection levels

We compared the spatial transcriptomes in each analysis cohort with the NCs and identified 41 unique or shared spatially differentially expressed transcripts associated with ND of SARS-CoV-2, SP, and HP detection of SARS-CoV-2 in the placenta (Figure 4A; Table S1, ST1.4). In mSARS-CoV-2$^+$ ND placentae, we did not observe inflammatory signaling cascades. Instead, we observed significant upregulation of *CSH2*, an isoform of placental lactogen, *GDF15*, a ligand of the transforming growth factor β (TGF-β) pathway, and KiSS-1 Metastasis Suppressor (*KISS1*). In both mSARS-CoV-2$^+$ ND and SP placentae, there was upregulation of pregnancy-specific β-1 glycoprotein 7 (*PSG7*). The 37 genes associated with HP SARS-CoV-2 in the placenta were analyzed by EnrichR[68,69] pathway analysis utilizing the Reactome 2022 database[70,71] (Figure 4B), revealing significant upregulation in interferon-stimulated genes (*ISG15*, *IFIT3*, and *IFITM3*), cytokines (*CXCL8*, *CXCL10*, and *CCL20*), and interleukin signaling (*ILR1L1*, *ILR1N*, *IL24*, and *IL32*). In addition, TIMP Metallopeptidase Inhibitor 1 (*TIMP1*) was a marker of highly positive SARS-CoV-2 placentae. Violin plots and spatial gene expression of *KISS1* and *TIMP1* (Figures 4C–4F) visualize the clear and significant upregulation of these markers in select mSARS-CoV-2$^+$ groups. Utilizing the term placenta atlas (Table S1, ST1.2), markers of ND mSARS-CoV-2$^+$ placentae *CSH2*, *KISS1*, and *GDF15* mapped to SYT cells, whereas cytokine markers of HP placentae mapped to immune cells and *TIMP1* mapped to fibroblasts and smooth muscle cells. Overall, the clusters from the sparsely positive or not detected groups were defined by canonical placental cell-type gene expression. In contrast, the clusters of spatial transcriptomes in the highly positive samples were characterized by different levels of antiviral responses and metallopeptidase signaling. The range in inflammation among HP niches, as well as the lack of inflammatory signaling in the ND and SP mSARS-CoV-2$^+$ cases, lends to an undefined dynamic separating inefficient and efficient SARS-CoV-2 replication in the placenta.

Patterns of inefficient and coordinated SARS-CoV-2 transcription gene expression in placental cells

Because SARS-CoV-2 viral replication in placental cells is relatively inefficient[17,72] and the Visium platform does not distinguish genomic SARS-CoV-2 from expressed transcripts, we examined patterns associated with the different levels of SARS-CoV-2 reads. The 752 spatial transcriptomes with detectable SARS-CoV-2 transcripts were subset, clustered, and further analyzed to assess differences in SARS-CoV-2 levels and potential viral gene expression (Figure 5). Viral transcripts per spot ranged from 1 to 1,554, with a mean of 18.9 and a median of 5.348 (raw counts in Table S1, ST1.5). Of the 752 spots with viral transcripts, 46.3% had ≥5, 219 spots had ≥10 (29%), 48 had ≥50 (6.4%), and 24 had ≥100 viral transcripts (3.2%). We performed pseudotime trajectory analysis[73–76] to identify relationships between these clusters (Figure 5A). To determine where the pseudotime trajectories should start, we examined the expression of viral RNAs in these clusters. Visualization of viral gene expression (Figure 5B) revealed ORF10 was expressed throughout all clusters, whereas ORF1ab was in clusters 2, 3, and 4, but not clusters 0 and 1. The mean counts of viral RNAs per cluster (Figure 5C) showed viral RNA levels ranked highest in cluster 1, followed by clusters 4, 2, and 0, and cluster 3 had the fewest. Utilizing this information, we started the pseudotime trajectories at cluster 3 because it had the lowest levels of viral transcripts (Figure 5D). We found two initial branchpoints, which either went up and ended at cluster 2 with low levels of viral transcripts, or another branchpoint that continued through clusters 0 and 4. This longer trajectory reached another branchpoint separating two distinct endpoints at cluster 0 or 1.

Next, we aimed to understand the differences between these distinct endpoints. Pearson's correlation analysis of all 752 viral transcriptomes, or analyzing subsets of cells within clusters, revealed significant positive correlation coefficients for ORF10 with N and ORF3A with ORF8 were observed only in the cluster with the highest amounts of viral RNA, cluster 1 (Figure 5E; Table S1, ST1.6), potentially representing a cascade of viral gene expression within these microenvironments. This was in contrast with the other clusters, which had no significant correlations in the co-expression of viral transcripts. These results demonstrated a range in SARS-CoV-2 gene expression efficiency within placental microenvironments and identified potential branchpoints where host-pathogen interactions may determine the trajectory of viral gene expression. To identify potential host-restriction factors, differential expression between clusters revealed upregulation of *CSH1* as a definitive marker for cluster 0, and a lack of *CSH1* was observed in clusters 2 and 3 (Table S1, ST1.6). Cluster 1 was marked by significant upregulation of SARS-CoV-2 N and the upregulation of 18 host transcripts, including *CXCL10*, *RACK1*, and *IFITM3*. Because cluster 1 had the highest viral RNA and was the cluster separating endpoints for clusters with low (cluster 0) and high viral RNA (cluster 4) with several branchpoints, these patterns of host and SARS-CoV-2 gene expression in cluster 1 are likely critical components of efficient SARS-CoV-2 gene expression in the placenta.

Tracing placental macrophage polarization trajectories reveals depletion of anti-inflammatory M2 macrophages and histiocytic intervillositis in highly positive SARS-CoV-2 placenta samples

To profile immune microenvironments, we turned to macrophage polarization marker transcripts (Figure 6; Figure S3). With a reductionist approach,[77] naive M0 macrophages exposed to polarization factors lead to pro-inflammatory M1 or anti-inflammatory M2 immunophenotypes (Figure 6A). We assessed the expression of known marker transcripts[78–87] for each of these subpopulations. The 3,180 placental macrophage niches were subset, and each macrophage cluster was annotated
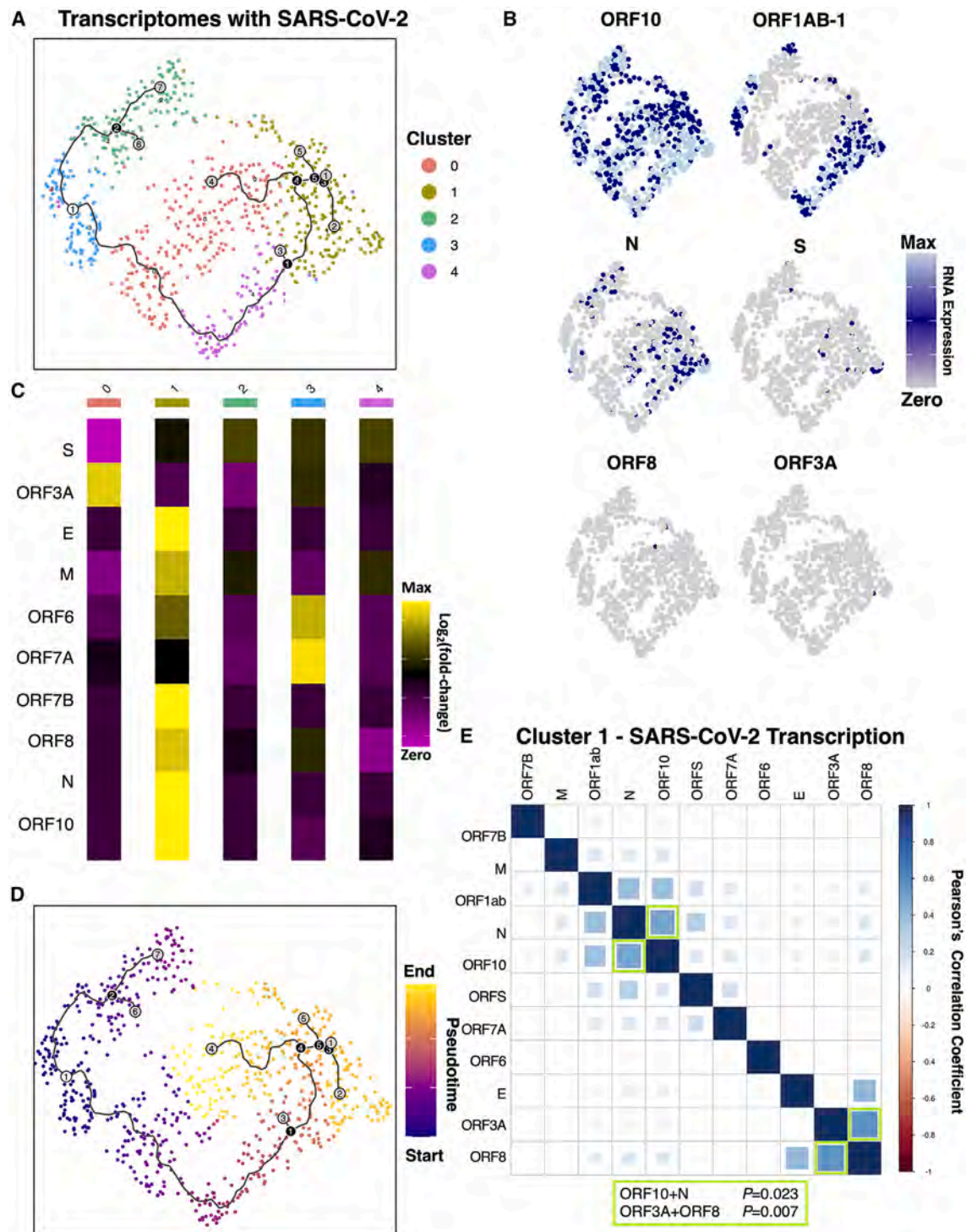
Figure 5. Analysis of infected spatial transcriptomes identifies distinct phases of inefficient and coordinated SARS-CoV-2 gene expression

(A) The 752 spatial transcriptomes with detectable SARS-CoV-2 transcripts were subset, clustered, and further analyzed. For continuity, the trajectories are plotted on (A) and (D), where the white circle represents the starting point, black circles represent branchpoints, and gray represents endpoints.

(B) Expression of viral transcripts revealed patterns in distinct clusters.

(C) The mean counts of viral RNAs per cluster revealed viral RNA levels were highest in clusters 1 > 4 > 2 > 0 > 3.

(D) Pseudotime trajectory analysis starting at cluster 3, which had the fewest viral transcripts, identified distinct endpoints at clusters 2, 0, and 1.

(E) Pearson's correlation analysis of each cluster revealed significant correlations in viral RNAs only in cluster 1.
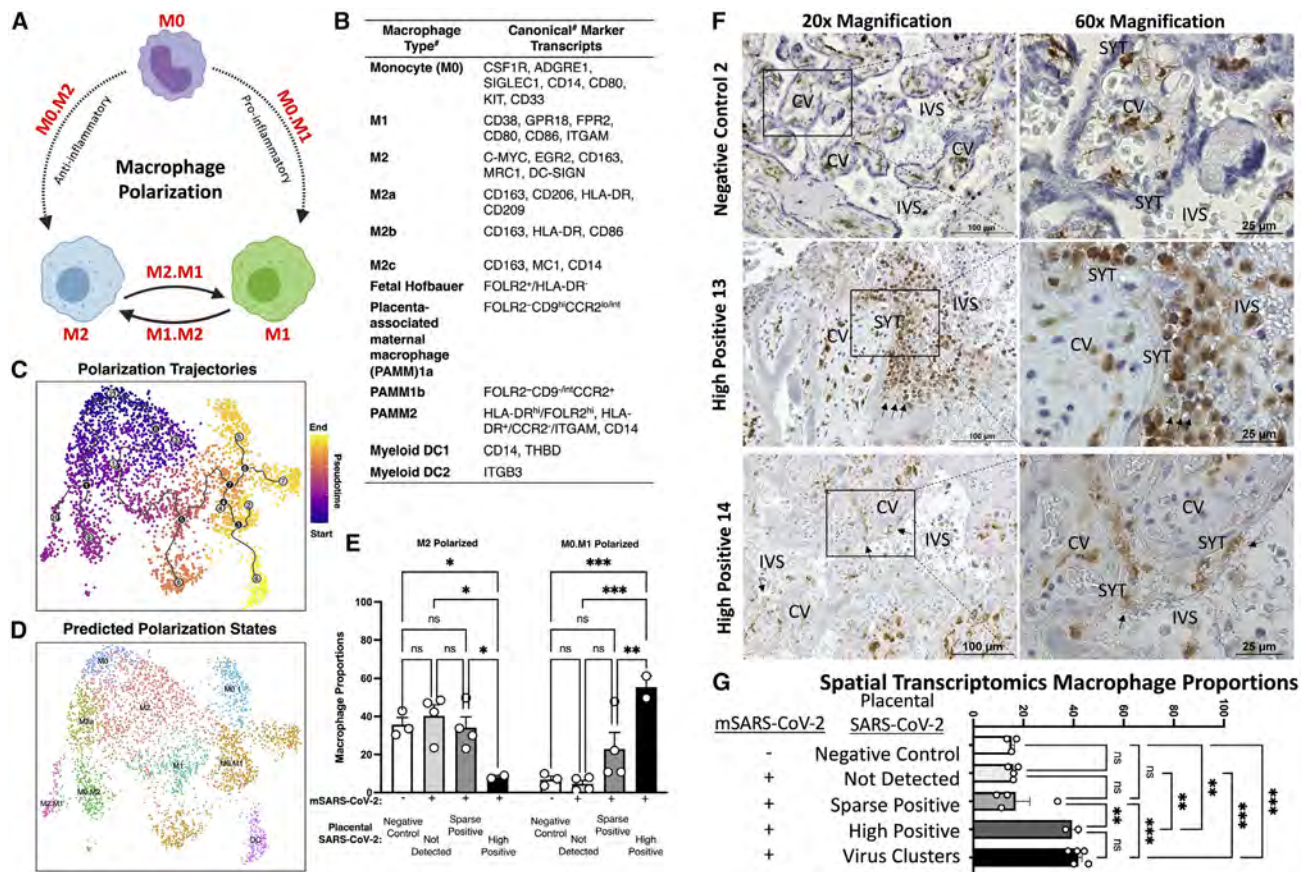
Figure 6. Tracing placental macrophage polarization trajectories identifies depletion of anti-inflammatory M2 macrophages and histiocytic intervillositis in highly positive SARS-CoV-2 placentae

(A) Schematic of macrophage polarization from naive monocytes (M0) to pro-inflammatory M1 and anti-inflammatory M2.

(B) Canonical markers for each subpopulation. #Caveats exist including potential differences by gestational age and between single-cell RNA and protein levels.

(C) The 3,180 placental macrophages were analyzed by Monocle3, revealing pseudotime trajectories starting at M0 monocytes and trajectories going to M1 or M2 polarized subpopulations.

(D) Using the pseudotime trajectory results, subpopulations were annotated based on predicted polarization states including intermediates (e.g., M0 to M1 is M0.M1).

(E) Proportions of macrophages according to predicted polarization states. Error bars represent the standard error of the mean.

(F and G) IHC staining for CD163, a classical macrophage marker. Images were taken at 40× original magnification. (G) Proportions of all spatial transcriptomes (see Figures 2 and S2C) were separated based on virus detection grouping from Figure 2 and the cluster analysis of SARS-CoV-2+ transcriptomes in Figure 5. Significance of $p < 0.05$ (**$p < 0.001$, ***$p < 0.0001$, ns$p > 0.05$) was determined by two-way ANOVA with Tukey's multiple comparisons test. Error bars represent the standard error of the mean.

based on the expression of polarization markers as either M0, M1, or M2. In addition, we aimed to distinguish fetal Hofbauer macrophage niches from placenta-associated maternal macrophage (PAMMs) niches based on specific expression of *FOLR2* present in the former and *HLA* in the latter,[87] although HLA expression increases in Hofbauer cells throughout gestation.[83] PAMMs, including PAMM2 subtypes, were in cluster 5, while the PAMM1 subtype was in macrophage cluster 6 (Figure S3), and Hofbauer cells were in clusters 0, 3, 4, 11, and 9. We did not observe significant differences between the proportion of PAMMs or Hofbauer microenvironments between samples at the spatial transcriptomics level. In turn, we focused on macrophage polarization utilizing pseudotime trajectory analysis[73,74,76] of the spatial transcriptomes. We identified subpopulations representative of branchpoint transitions between M0 and the M1 or M2 polarization states, which

we denoted as M0.M1 or M0.M2. Differential expression between polarization states identified unique transcription programs associated with the branch and endpoints for each polarization state (Table S1, ST1.7). In the highly positive SARS-CoV-2 placenta samples, we found a significant decrease in the proportion of M2 polarized macrophages and a significant increase in M0.M1 transition macrophages (*$p < 0.05$; two-way ANOVA with Tukey's multiple comparisons test). The transitory M0.M1 macrophages did not exhibit PAMM or Hofbauer cell markers, but most M2 macrophages exhibited Hofbauer cell marker expression, consistent with their normal anti-inflammatory functions. These differences in macrophage polarization were not significant based on fetal sex or in comparisons between sparsely SARS-CoV-2$^+$ placentae.

To determine whether increased macrophage infiltration was associated with SARS-CoV-2 placental replication and histopathology, we stained for the canonical macrophage marker CD163 by IHC (Figure 6F). In HP13 and HP14, we found evidence of histiocytic intervillositis, detailed by high levels of macrophages localizing in the intervillous space, adjacent to the SYT layers comprising the maternal-fetal interface. To contextualize the results of histiocytic intervillositis in the highly positive SARS-CoV-2 placentae with the spatial transcriptomics analysis, we compared relative macrophage proportions in the spatial transcriptomics groups (Figure 6G). We found macrophage proportions of the highly positive samples (HP13 and HP14) were significantly higher than the other analysis cohorts. Also, we found macrophage proportions were significantly elevated in all the clusters with various levels of SARS-CoV-2 RNA analyzed in Figure 5. Because all the virus clusters had increased macrophage proportions, this increase was independent of the low or high levels of SARS-CoV-2. Together, these data suggest a potential threshold of SARS-CoV-2 positivity within the placenta before histiocytic intervillositis.

Fetal sex differences in gene expression responses associated with SARS-CoV-2 mapped to the fetal space in females and maternal decidua in males

Because the placenta is composed of both maternal (minority in bulk) and fetal (majority) cells, caution was needed in parsing by fetal sex. Spatial resolution allowed for key biologic distinctions, because mapping potential changes in gene expression back to the anatomical regions would reveal confounders of maternal cells in the decidual region. We performed differential expression between placentae from male and female fetuses in the SARS-CoV-2 scRNA-seq data (147,906 transcriptomes[19]), revealing the most significant genes were in VCT, stromal, and smooth muscle cells (Figure S4A). Analysis of the 9,446 mSARS-CoV-2 placenta spatial transcriptomes revealed fetal sex differences in gene expression in VCTs, macrophages, and EVT niches (Figure S4C). EVT spatial transcriptomes were mapped to regions of maternal decidua (Figure 2D). This highlights the importance of spatial resolution, which permits the assignment of fetal sex differences in gene expression to distinct fetal (chorionic villi) or maternal (decidua) regions.

To enhance rigor and reproducibility, we subjected the 208 significantly ($q < 0.05$) differentially expressed genes in the SARS-CoV-2 scRNA-seq (147,906 transcriptomes[19]) and spatial transcriptomics (9,446 transcriptomes) data based on fetal sex to EnrichR[68] pathway analysis using the BioPlanet[69] database. The top 90th quartile of significant ($q < 0.05$) pathways included T cell receptor regulation of apoptosis, interferon signaling, prolactin, and cytokine regulation (Figure 7A). Although T cell receptor regulation of apoptosis was the most significant pathway of these genes with fetal sex differences in expression, we did not find placental spatial transcriptomes resembling T cell expression profiles. However, the genes
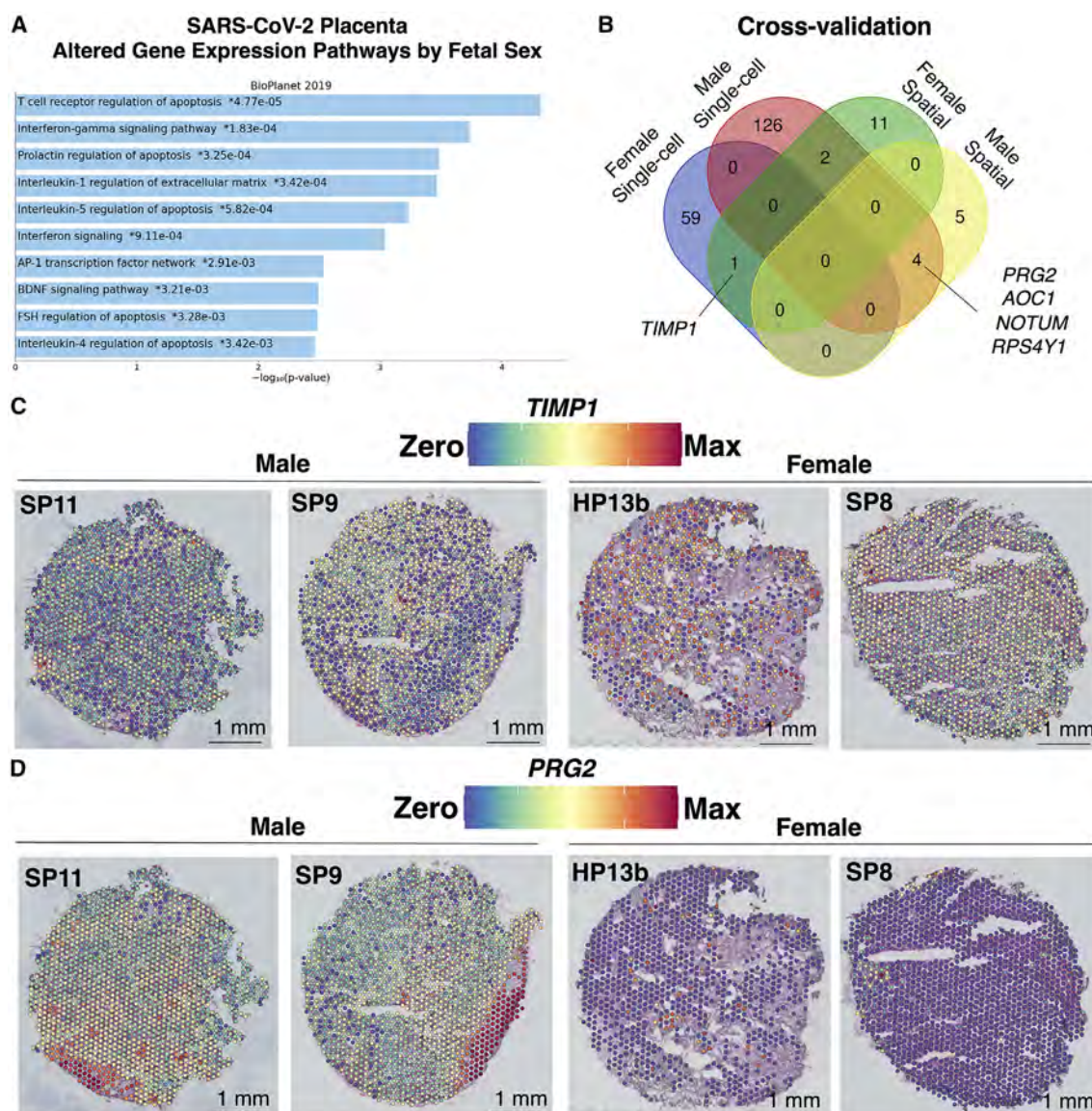
Figure 7. Caution in assigning fetal sex differences in gene expression associated with placental SARS-CoV-2 without spatial resolution

(A) The 208 significantly (q < 0.05) differentially expressed genes in the SARS-CoV-2 scRNA-seq (147,906 transcriptomes; n = 15 female and 30 male)[19] and spatial transcriptomics (9,446 transcriptomes; n = 4 male and 5 female) data based on fetal sex were uploaded to EnrichR for BioPlanet pathway analysis. The top 90th quartiles of most significant (q < 0.05) pathways were plotted.

(B) The 208 genes with sex differences in expression from the SARS-CoV-2 scRNA-seq and spatial transcriptomics datasets were compared and plotted as a Venn diagram, revealing four male and one female cross-validated gene.

(C and D) Spatial gene expressions of cross-validated genes (C) TIMP1 and (D) PRG2 were upregulated in the villous space in females and maternal decidua regions of male SARS-CoV-2 placentae, respectively.

highlighted in this pathway included *RPS4Y1* (Y chromosome linked), in addition to *GBP1* and *HSPA1A* (expressed in macrophages), and *HLA-G* (highly expressed in trophoblasts subtypes). These 208 genes with fetal sex differences in expression from the SARS-CoV-2 scRNA-seq and spatial transcriptomics datasets were compared and plotted as a Venn diagram, revealing four high-confidence genes with fetal sex differences in expression with male fetuses and one cross-validated gene with female fetuses. Spatial gene expression of cross-validated *TIMP1* and *PRG2* transcripts projected these putative genes with fetal sex differences in

expression onto male and female placentae (Figures 7C and 7D). Based on the term placenta transcriptomic atlas (Figure 2), *TIMP1* expression was upregulated in fibroblasts and smooth muscle cells and mapped to chorionic villi. In contrast, *PRG2* was upregulated in EVTs, cells known to invade the maternal decidua. Together, these data suggest genes with fetal sex differences in expression mapped specifically to the maternal decidua in males and fetal spaces in females may contribute to differences in T cell function and recruitment in response to SARS-CoV-2 in the placenta.

DISCUSSION

Principal findings

This study advances placental biology by generating a high-resolution term placental atlas using single-cell, single-nuclei, and spatial transcriptomics in coordinated analyses. With these rigorous and highly sensitive orthogonal approaches, SARS-CoV-2 was detected in 7 of 10 mSARS-CoV-2^{+} placentae, ranging from high levels of SARS-CoV-2 found in two IUFD samples (HP13 and HP14) to the detection of sparse SARS-CoV-2 RNA in five samples (SP8–SP12) and no detection in three. We found immune microenvironments largely sequestered SARS-CoV-2 in placental tissue localized to SYT cells and associated with increased macrophage infiltration. With spatial transcriptomics, this was associated with a depletion of anti-inflammatory M2 macrophages, paired with increases in pro-inflammatory M0.M1 transitory macrophages. The maternal COVID-19 symptoms in both IUFD cases HP13 and HP14 started and ended 5–10 days before the IUFD was detected, indicating prolonged SARS-CoV-2 infection of the placenta may have been a contributing factor to fetal pathogenesis. Together, this high-molecular- resolution study from a small but clinically diverse cohort of participants suggests that simultaneous host-pathogen battlegrounds lead to the clearance of sparse SARS-CoV-2 placental infections and identifies potential SARS-CoV-2 niches that persist up to 10 days after the onset and resolution of symptoms.

Detection of sparse SARS-CoV-2 transcripts in placentae using high-resolution spatial transcriptomics

Tracking SARS-CoV-2 prevalence in placental tissues has been technically challenging and limited by the sensitivity of detection.[19,65] The early detection of SARS-CoV-2 infection of placental tissue and maternal-fetal vertical transmission was put in doubt, partly because of the low prevalence initially[10] and the presumed absence of SARS-CoV-2 entry receptor *ACE2* and co-factor *TMPRSS2* co-expression in single-cell placenta data.[34,88,89] Of the 752 spatial transcriptomes with SARS-CoV-2 viral transcripts, none of these spots had *ACE2* or *TMPRSS2* expression, potentially highlighting known[90] discordance between RNA expression and protein levels. Recently, SARS-CoV-2 was shown to spread by cell-to-cell fusion in the absence of *ACE2* receptors,[91] which could explain the viral spread observed in placental tissue and the broad tropism of SARS-CoV-2.[92,93] Notably, in the cohort of placentae analyzed here, there was no evidence of vertical transmission of SARS-CoV-2 to the offspring. Yet, even in the absence of transplacental vertical transmission, the presence of particular microbes at the maternal-fetal interface may have detrimental impacts on the fetal immune responses, including increased inflammatory signaling and developmental disorders.[53,94,95] The rates of SARS-CoV-2 in the placentae included in this cohort were high (7 of 10) relative to prior studies[65,96] that analyzed more cases, and reported rates ranging from 7% to 15%. This could potentially be caused by the inclusion of both symptomatic and asymptomatic mSARS-CoV-2^{+} cases, the complementary orthogonal bulk and high-resolution assays included here, or the collection of these specimens during the Delta variant surge.

A model of dynamic SARS-CoV-2 placental infection

The data in this study support a model of SARS-CoV-2 placental infection with three likely endpoints. First, SARS-CoV-2 frequently does not reach or enter placental cells and is cleared prior to infiltrating beyond the maternal-fetal interface (no virus detected in 3 of 10 mSARS-CoV-2$^+$ samples). Second, with high-resolution orthogonal approaches, sparse levels of SARS-CoV-2 may be commonly detected in placental cells in association with inefficient viral replication, and an appropriate immune response limits inflammatory signaling. Third, in rare cases, efficient SARS-CoV-2 replication in the placenta may break a threshold of host-pathogen equilibrium associated with hallmark histopathologies such as inflammation, histiocytic intervillositis, and perivillous fibrinoid deposition. Notably, the proposed phases of SARS-CoV-2 placental infection account for the dynamics of asymptomatic mSARS-CoV-2 positivity and maternal COVID-19.

Dynamic range of SARS-CoV-2 responses in placental microenvironments

We found placental markers associated with inefficient SARS-CoV-2 in the placenta (ND and SP) and highly efficient SARS-CoV-2 replication (HP) in the placenta (Figure 3A). Inefficient SARS-CoV-2 in the placenta was associated with *KISS1*, *GDF15*, and *CSH2* markers in SYT niches. *KISS1* is associated with decidualization,[97] *GDF15* is an effector in the TGF-β pathway and associated with reducing tissue damage,[98] and *CSH2* is an isoform of placental lactogen with multiple roles in fetal metabolism.[99] In both ND and SP mSARS-CoV-2$^+$ placentae, *PSG7* was upregulated. In trophoblast cultures, exposures to hypoxic and pro-inflammatory conditions were inversely correlated with PSG7 mRNA and protein levels.[100] Together, we speculate these ND and SP signatures represented the sequestration of antiviral responses to confined microenvironments.

In contrast, the signatures of high SARS-CoV-2 levels in the placenta were associated with a dynamic range of hyper-inflammation and tissue damage. Comparisons of two sections from the same highly positive placenta (Figure 3B) revealed 5% of spatial transcriptomes in HP13a had SARS-CoV-2, whereas over 86% of spots in HP13b had SARS-CoV-2. This range was associated with histopathology because HP13a had perivillous fibrinoids, whereas HP13b did not. We posit these microenvironments were associated with a critical threshold separating inefficient and efficient SARS-CoV-2 replication in the placenta, and we aimed to identify genes critical to maintaining or surpassing these thresholds. A cluster with coordinated viral transcription (Figure 5, cluster 1) was marked by significant upregulation of 18 host transcripts, including *CXCL10*, *RACK1*, and *IFITM3*. These host genes are now known to be critical factors for SARS-CoV-2 cytokine storm,[101–106] enhancing viral replication,[107] and restricting SARS-CoV-2 spread through cell-to-cell fusion.[18,108–110] In addition, the progression of placental SARS-CoV-2 infection potentially co-opted components of extracellular matrix restructuring. *TIMP1* was a spatial marker of SARS-CoV-2 (Figure 4) and gene upregulated in the fetal villi space in female placentae (Figure 7). Recently, increased serum levels of *TIMP1* significantly correlated with COVID-19 severity.[111] In addition, a recent *in vitro* study found that Delta variant SARS-CoV-2 spike protein utilizes matrix metalloproteinases (MMPs) as an alternative to co-factor *TMPRSS2* for viral entry, and in turn, metalloproteinase inhibitors limited cell-cell fusion and viral replication.[112] This is perhaps not surprising, because viral adaptation to a novel host is likely to occur concomitantly with extracellular matrix restructuring and macrophage migration. In the placental tissue, the presence of histopathologic findings consistent with these processes (perivillous fibrin deposition and histiocytic intervillous changes) suggests a balance between MMPs and *TIMP1* may be critical to modulating

placental SARS-CoV-2 entry and replication with viral-mediated catastrophic placental destruction. *TIMP1* is encoded on the X chromosome and has previously been linked to a sex disparity in liver and pancreatic cancers,[113] but the potential sex differences in gene expression for *TIMP1* in the recruitment of T and macrophage cells to the maternal decidua warrant further investigation.

Term placenta transcriptomic atlas with single-cell and spatial resolution

In addition to providing a benchmark for comparison between placenta single-cell, single-nuclei, and spatial transcriptomics analyses, the term placenta transcriptomic atlas aids the field by allowing any gene of interest to be mapped to specific regions of the placenta (maternal decidua, chorionic villi, basal plate, or chorioamniotic membranes) and 22 distinct cell populations. For example, the term placenta atlas allows comparisons of subjects with gestational diabetes mellitus (GDM), pre-eclampsia, SARS-CoV-2 asymptomatic, SARS-CoV-2 symptomatic, and SARS-CoV-2 (symptoms unknown). Relative to the pooled healthy controls, we identified gene signatures associated with each condition (Table S1, ST1.2). There were 72 significantly differentially expressed genes among these conditions, including heat shock proteins as top markers of GDM, consistent with previous findings,[114] and these changes associated with GDM mapped specifically to macrophage and endothelial niches (Table S1, ST1.2).

Conclusions

Spatial transcriptomics of placentae collected during the Delta variant surge, when the burden on the maternal-fetal health was at its peak, characterized distinct niches in the maternal and fetal spaces of the placenta and captured differences ranging from healthy uninfected placentae to highly SARS-CoV-2 placentae from an IUFD case. In the worst-case scenario, we observed massive inflammation, which led to perivillous fibrin deposition. However, in the mSARS-CoV-2$^+$ placentae, where SARS-CoV-2 was not detected or sparse, we did not observe coordinated pro-inflammatory signaling. Therefore, in most cases, the placenta likely responds to SARS-CoV-2 and other intrauterine microbes with immune microenvironments in order to sequester inflammatory signaling and limit tissue damage. Recent autopsies of non-pregnant persons found SARS-CoV-2 may persist for up to 7 months in a wide range of tissues.[93,115] A robust high-resolution prospective study of asymptomatic and symptomatic SARS-CoV-2 detection during pregnancy compared with longitudinal viral persistence in placental tissues is warranted.

Limitations of the study

HP13 was a preterm (22.3 weeks' gestation) case where the mother was COVID-19 symptomatic and recovered over 10 days, after which IUFD was observed. We were not powered to assess the influence of gestational age.[116–125] To enhance rigor and reproducibility, we histopathologically examined HP14, an additional IUFD placenta (35.0 weeks' gestation). HP14 exhibited SARS-CoV-2 histological results aligning with HP13, including perivillous fibrinoid deposition, high amounts of spike RNA by RNAscope, spike and nucleocapsid protein in the SYT layer, and increased macrophage histiocytic intervillositis. The observations of sparse viral microenvironments of one viral transcript in SP11 and one in SP12 (Figure 3) suggest the limit of detection for SARS-CoV-2 in placentae by spatial transcriptomics is 1 in 700 cells, which was a higher resolution than bulk RT-qPCR (1 in 7,000 cells). Both techniques have limitations considering the low biomass of SARS-CoV-2 genomic and transcribed RNA (2.9 kb/copy) compared with an estimated average of 10,000,000 host RNA molecules per mammalian cell.[126]

STAR★METHODS

Detailed methods are provided in the online version of this paper and include the following:

- KEY RESOURCES TABLE
- RESOURCE AVAILABILITY
  - Lead contact
  - Materials availability
  - Data and code availability
- EXPERIMENTAL MODEL AND STUDY PARTICIPANT DETAILS
  - Study approval
- METHOD DETAILS
  - Spatial transcriptomics
  - Single-cell and spatial transcriptomics analyses
  - RT-qPCR
  - RNAscope
  - Immunohistochemistry
- QUANTIFICATION AND STATISTICAL ANALYSIS
  - Statistics

SUPPLEMENTAL INFORMATION

Supplemental information can be found online at https://doi.org/10.1016/j.medj.2023.06.003.

AUTHOR CONTRIBUTIONS

Experimental design: E.R.B., E.C.C.C., M.D.S., A.M.M., M.D.J., R.F.R., C.D.S., and K.M.A.; tissue acquisition: R.F.R., E.C.C.C., M.D.S., E.R.B., and K.M.A.; data curation: E.R.B., E.C.C.C., A.M.M., M.D.S., M.D.J., and K.M.A.; data analysis: E.R.B., E.C.C.C., M.D.S., M.D.J., and K.M.A.; interpretation: E.R.B., E.C.C.C., A.M.M., M.D.S., M.D.J., R.F.R., and K.M.A.; writing the manuscript: E.R.B., E.C.C.C., M.D.S., M.D.J., C.D.S., and K.M.A.; manuscript revisions: E.R.B., E.C.C.C., A.M.M., M.D.S., M.D.J., R.F.R., C.D.S., and K.M.A.; and funding: E.R.B. and K.A.M.

DECLARATION OF INTERESTS

The authors declare no competing interests.

INCLUSION AND DIVERSITY

We support inclusive, diverse, and equitable conduct of research. One or more of the authors of this paper self-identifies as an underrepresented ethnic minority in their field of research or within their geographical location. One or more of the authors of this paper received support from a program designed to increase minority representation in their field of research.

REFERENCES

1. Boyton, R.J., and Altmann, D.M. (2021). The immunology of asymptomatic SARS-CoV-2 infection: what are the key questions? Nat. Rev. Immunol. *21*, 762–768. https://doi.org/10.1038/s41577-021-00631-x.

2. Oran, D.P., and Topol, E.J. (2020). Prevalence of asymptomatic SARS-CoV-2 infection : a narrative review. Ann. Intern. Med. *173*, 362–367. https://doi.org/10.7326/M20-3012.

3. Oran, D.P., and Topol, E.J. (2021). The proportion of SARS-CoV-2 infections that are asymptomatic : a systematic review. Ann. Intern. Med. *174*, 655–662. https://doi.org/10.7326/M20-6976.

4. Vousden, N., Bunch, K., Morris, E., Simpson, N., Gale, C., O'Brien, P., Quigley, M., Brocklehurst, P., Kurinczuk, J.J., and Knight, M. (2021). The incidence, characteristics and outcomes of pregnant women hospitalized with symptomatic and asymptomatic SARS-CoV-2 infection in the UK from March to September 2020: a national cohort study using the UK Obstetric Surveillance System (UKOSS). PLoS One *16*, e0251123. https://doi.org/10.1371/journal.pone.0251123.

5. Cruz-Lemini, M., Ferriols Perez, E., de la Cruz Conty, M.L., Cano Aguilar, A., Encinas Pardilla, M.B., Prats Rodriguez, P., Muner Hernando, M., Forcen Acebal, L., Pintado Recarte, P., Medina Mallen, M.D.C., et al. (2021). Obstetric outcomes of SARS-CoV-2 infection in asymptomatic pregnant women. Viruses *13*, 112. https://doi.org/10.3390/v13010112.

6. De Biasi, S., Tartaro, D.L., Gibellini, L., Paolini, A., Quong, A., Petes, C., Awong, G., Douglas, S., Lin, D., Nieto, J., et al. (2021). Endogenous control of inflammation characterizes pregnant women with asymptomatic or paucisymptomatic SARS-CoV-2 infection. Nat. Commun. *12*, 4677. https://doi.org/10.1038/s41467-021-24940-w.

7. Hantoushzadeh, S., Shamshirsaz, A.A., Aleyasin, A., Seferovic, M.D., Aski, S.K., Arian, S.E., Pooransari, P., Ghotbizadeh, F., Aalipour, S., Soleimani, Z., et al. (2020). Maternal death due to COVID-19. Am. J. Obstet. Gynecol. *223*. https://doi.org/10.1016/j.ajog.2020.04.030.

8. Preis, H., Mahaffey, B., Heiselman, C., and Lobel, M. (2020). Vulnerability and resilience to pandemic-related stress among U.S. women pregnant at the start of the COVID-19 pandemic. Soc. Sci. Med. *266*, 113348. https://doi.org/10.1016/j.socscimed.2020.113348.

9. Stratton, P., Gorodetsky, E., and Clayton, J. (2021). Pregnant in the United States in the COVID-19 pandemic: a collision of crises we cannot ignore. J. Natl. Med. Assoc. *113*, 499–503. https://doi.org/10.1016/j.jnma.2021.03.008.

10. Chen, H., Guo, J., Wang, C., Luo, F., Yu, X., Zhang, W., Li, J., Zhao, D., Xu, D., Gong, Q., et al. (2020). Clinical characteristics and intrauterine vertical transmission potential of COVID-19 infection in nine pregnant women: a retrospective review of medical records. Lancet *395*, 809–815. https://doi.org/10.1016/S0140-6736(20)30360-3.

11. Debelenko, L., Katsyv, I., Chong, A.M., Peruyero, L., Szabolcs, M., and Uhlemann, A.C. (2021). Trophoblast damage with acute and chronic intervillositis: disruption of the placental barrier by severe acute respiratory syndrome coronavirus 2. Hum. Pathol. *109*, 69–79. https://doi.org/10.1016/j.humpath.2020.12.004.

12. Shamshirsaz, A.A., Hessami, K., Morain, S., Afshar, Y., Nassr, A.A., Arian, S.E., Asl, N.M., and Aagaard, K. (2022). Intention to receive COVID-19 vaccine during pregnancy: a systematic review and meta-analysis. Am. J. Perinatol. *39*, 492–500. https://doi.org/10.1055/a-1674-6120.

13. Research Committee; Society for Maternal-Fetal Medicine SMFM, Boelig, R.C., Aagaard, K.M., Debbink, M.P., and Shamshirsaz, A.A.; SMFM Research Committee Electronic address smfm@smfmorg (2021). Society for maternal-fetal medicine special statement: COVID-19 research in pregnancy: progress and potential. Am. J. Obstet. Gynecol. *225*, B19–B31. https://doi.org/10.1016/j.ajog.2021.08.039.

14. Sapoval, N., Mahmoud, M., Jochum, M.D., Liu, Y., Elworth, R.A.L., Wang, Q., Albin, D., Ogilvie, H.A., Lee, M.D., Villapol, S., et al. (2021). SARS-CoV-2 genomic diversity and the implications for qRT-PCR diagnostics and transmission. Genome Res. *31*, 635–644. https://doi.org/10.1101/gr.268961.120.

15. Sulentic, R.O., Seferovic, M.D., Aagaard, K.M., and Valentine, G.C. (2022). Perinatal COVID-19 outcomes: evaluating the strength of current evidence. J. Matern. Fetal Neonatal Med. *35*, 4250–4257. https://doi.org/10.1080/14767058.2020.1849101.

16. Vivanti, A.J., Vauloup-Fellous, C., Prevot, S., Zupan, V., Suffee, C., Do Cao, J., Benachi, A., and De Luca, D. (2020). Transplacental transmission of SARS-CoV-2 infection. Nat. Commun. *11*, 3572. https://doi.org/10.1038/s41467-020-17436-6.

17. Tallarek, A.C., Urbschat, C., Fonseca Brito, L., Stanelle-Bertram, S., Krasemann, S., Frascaroli, G., Thiele, K., Wieczorek, A., Felber, N., Lütgehetmann, M., et al. (2021). Inefficient placental virus replication and absence of neonatal cell-specific immunity upon sars-CoV-2 infection during pregnancy. Front. Immunol. *12*, 698578. https://doi.org/10.3389/fimmu.2021.698578.

18. Mourad, M., Jacob, T., Sadovsky, E., Bejerano, S., Simone, G.S.D., Bagalkot, T.R., Zucker, J., Yin, M.T., Chang, J.Y., Liu, L., et al. (2021). Placental response to maternal SARS-CoV-2 infection. Sci. Rep. *11*, 14390. https://doi.org/10.1038/s41598-021-93931-0.

19. Garcia-Flores, V., Romero, R., Xu, Y., Theis, K.R., Arenas-Hernandez, M., Miller, D., Peyvandipour, A., Bhatti, G., Galaz, J., Gershater, M., et al. (2022). Maternal-fetal immune responses in pregnant women infected with SARS-CoV-2. Nat. Commun. *13*, 320. https://doi.org/10.1038/s41467-021-27745-z.

20. Hessami, K., Aagaard, K.M., Castro, E.C., Arian, S.E., Nassr, A.A., Barrozo, E.R., Seferovic, M.D., and Shamshirsaz, A.A. (2022). Placental vascular and inflammatory findings from pregnancies diagnosed with coronavirus disease 2019 (COVID-19): a systematic review

and meta-analysis. Am. J. Perinatol. *39*, 1643–1653. https://doi.org/10.1055/a-1787-7933.

21. Sureshchandra, S., Zulu, M.Z., Doratt, B.M., Jankeel, A., Tifrea, D., Edwards, R., Rincon, M., Marshall, N.E., and Messaoudi, I. (2022). Single-cell RNA sequencing reveals immunological rewiring at the maternal-fetal interface following asymptomatic/mild SARS-CoV-2 infection. Cell Rep. *39*, 110938. https://doi.org/10.1016/j.celrep.2022.110938.

22. Lesseur, C., Jessel, R.H., Ohrn, S., Ma, Y., Li, Q., Dekio, F., Brody, R.I., Wetmur, J.G., Gigase, F.A.J., Lieber, M., et al. (2022). Gestational SARS-CoV-2 infection is associated with placental expression of immune and trophoblast genes. Placenta *126*, 125–132. https://doi.org/10.1016/j.placenta.2022.06.017.

23. Taglauer, E., Benarroch, Y., Rop, K., Barnett, E., Sabharwal, V., Yarrington, C., and Wachman, E.M. (2020). Consistent localization of SARS-CoV-2 spike glycoprotein and ACE2 over TMPRSS2 predominance in placental villi of 15 COVID-19 positive maternal-fetal dyads. Placenta *100*, 69–74. https://doi.org/10.1016/j.placenta.2020.08.015.

24. Male, V. (2022). SARS-CoV-2 infection and COVID-19 vaccination in pregnancy. Nat. Rev. Immunol. *22*, 277–282. https://doi.org/10.1038/s41577-022-00703-6.

25. Ruan, D., Ye, Z.W., Yuan, S., Li, Z., Zhang, W., Ong, C.P., Tang, K., Ka Ki Tam, T.T., Guo, J., Xuan, Y., et al. (2022). Human early syncytiotrophoblasts are highly susceptible to SARS-CoV-2 infection. Cell Rep. Med. *3*, 100849. https://doi.org/10.1016/j.xcrm.2022.100849.

26. Fahmi, A., Brügger, M., Démoulins, T., Zumkehr, B., Oliveira Esteves, B.I., Bracher, L., Wotzkow, C., Blank, F., Thiel, V., Baud, D., and Alves, M.P. (2021). SARS-CoV-2 can infect and propagate in human placenta explants. Cell Rep. Med. *2*, 100456. https://doi.org/10.1016/j.xcrm.2021.100456.

27. Bost, P., Giladi, A., Liu, Y., Bendjelal, Y., Xu, G., David, E., Blecher-Gonen, R., Cohen, M., Medaglia, C., Li, H., et al. (2020). Host-viral infection maps reveal signatures of severe COVID-19 patients. Cell *181*, 1475–1488.e12. https://doi.org/10.1016/j.cell.2020.05.006.

28. Ren, X., Wen, W., Fan, X., Hou, W., Su, B., Cai, P., Li, J., Liu, Y., Tang, F., Zhang, F., et al. (2021). COVID-19 immune features revealed by a large-scale single-cell transcriptome atlas. Cell *184*, 1895–1913.e19. https://doi.org/10.1016/j.cell.2021.01.053.

29. Zhang, J.Y., Wang, X.M., Xing, X., Xu, Z., Zhang, C., Song, J.W., Fan, X., Xia, P., Fu, J.L., Wang, S.Y., et al. (2020). Single-cell landscape of immunological responses in patients with COVID-19. Nat. Immunol. *21*, 1107–1118. https://doi.org/10.1038/s41590-020-0762-x.

30. Wilk, A.J., Rustagi, A., Zhao, N.Q., Roque, J., Martínez-Colón, G.J., McKechnie, J.L., Ivison, G.T., Ranganath, T., Vergara, R., Hollis, T., et al. (2020). A single-cell atlas of the peripheral immune response in patients with severe COVID-19. Nat. Med. *26*, 1070–1076. https://doi.org/10.1038/s41591-020-0944-y.

31. Melms, J.C., Biermann, J., Huang, H., Wang, Y., Nair, A., Tagore, S., Katsyv, I., Rendeiro, A.F., Amin, A.D., Schapiro, D., et al. (2021). A molecular single-cell lung atlas of lethal COVID-19. Nature *595*, 114–119. https://doi.org/10.1038/s41586-021-03569-1.

32. Guo, C., Li, B., Ma, H., Wang, X., Cai, P., Yu, Q., Zhu, L., Jin, L., Jiang, C., Fang, J., et al. (2020). Single-cell analysis of two severe COVID-19 patients reveals a monocyte-associated and tocilizumab-responding cytokine storm. Nat. Commun. *11*, 3924. https://doi.org/10.1038/s41467-020-17834-w.

33. Ziegler, C.G.K., Allon, S.J., Nyquist, S.K., Mbano, I.M., Miao, V.N., Tzouanas, C.N., Cao, Y., Yousif, A.S., Bals, J., Hauser, B.M., et al. (2020). SARS-CoV-2 receptor ACE2 is an interferon-stimulated gene in human airway epithelial cells and is detected in specific cell subsets across tissues. Cell *181*, 1016–1035.e19. https://doi.org/10.1016/j.cell.2020.04.035.

34. Pique-Regi, R., Romero, R., Tarca, A.L., Luca, F., Xu, Y., Alazizi, A., Leng, Y., Hsu, C.D., and Gomez-Lopez, N. (2020). Does the human placenta express the canonical cell entry mediators for SARS-CoV-2? Elife *9*, e58716. https://doi.org/10.7554/eLife.58716.

35. Li, M., Chen, L., Zhang, J., Xiong, C., and Li, X. (2020). The SARS-CoV-2 receptor ACE2 expression of maternal-fetal interface and fetal organs by single-cell transcriptome study. PLoS One *15*, e0230295. https://doi.org/10.1371/journal.pone.0230295.

36. Ashary, N., Bhide, A., Chakraborty, P., Colaco, S., Mishra, A., Chhabria, K., Jolly, M.K., and Modi, D. (2020). Single-cell RNA-seq identifies cell subsets in human placenta that highly expresses factors driving pathogenesis of SARS-CoV-2. Front. Cell Dev. Biol. *8*, 783. https://doi.org/10.3389/fcell.2020.00783.

37. Cui, D., Liu, Y., Jiang, X., Ding, C., Poon, L.C., Wang, H., and Yang, H. (2021). Single-cell RNA expression profiling of SARS-CoV-2-related ACE2 and TMPRSS2 in human trophectoderm and placenta. Ultrasound Obstet. Gynecol. *57*, 248–256.

38. Lu-Culligan, A., Chavan, A.R., Vijayakumar, P., Irshaid, L., Courchaine, E.M., Milano, K.M., Tang, Z., Pope, S.D., Song, E., Vogels, C.B.F., et al. (2021). Maternal respiratory SARS-CoV-2 infection in pregnancy is associated with a robust inflammatory response at the maternal-fetal interface. Med *2*, 591–610.e10. https://doi.org/10.1016/j.medj.2021.04.016.

39. Chen, J., Du, L., Wang, F., Shao, X., Wang, X., Yu, W., Bi, S., Chen, D., Pan, X., Zeng, S., et al. (2022). Cellular and molecular atlas of the placenta from a COVID-19 pregnant woman infected at midgestation highlights the defective impacts on foetal health. Cell Prolif. *55*, e13204. https://doi.org/10.1111/cpr.13204.

40. Matute, J.D., Finander, B., Pepin, D., Ai, X., Smith, N.P., Li, J.Z., Edlow, A.G., Villani, A.C., Lerou, P.H., and Kalish, B.T. (2022). Single-cell immunophenotyping of the fetal immune response to maternal SARS-CoV-2 infection in late gestation. Pediatr. Res. *91*, 1090–1098. https://doi.org/10.1038/s41390-021-01793-z.

41. Bordt, E.A., Shook, L.L., Atyeo, C., Pullen, K.M., De Guzman, R.M., Meinsohn, M.C., Chauvin, M., Fischinger, S., Yockey, L.J., James, K., et al. (2021). Maternal SARS-CoV-2 infection elicits sexually dimorphic placental immune responses. Sci. Transl. Med. *13*, eabi7428. https://doi.org/10.1126/scitranslmed.abi7428.

42. Argueta, L.B., Lacko, L.A., Bram, Y., Tada, T., Carrau, L., Rendeiro, A.F., Zhang, T., Uhl, S., Lubor, B.C., Chandar, V., et al. (2022). Inflammatory responses in the placenta upon SARS-CoV-2 infection late in pregnancy. iScience *25*, 104223. https://doi.org/10.1016/j.isci.2022.104223.

43. Schwartz, D.A., Baldewijns, M., Benachi, A., Bugatti, M., Bulfamante, G., Cheng, K., Collins, R.R.J., Debelenko, L., De Luca, D., Facchetti, F., et al. (2021). Hofbauer cells and COVID-19 in pregnancy. Arch. Pathol. Lab Med. *145*, 1328–1340. https://doi.org/10.5858/arpa.2021-0296-SA.

44. Steel, J.H., Malatos, S., Kennea, N., Edwards, A.D., Miles, L., Duggan, P., Reynolds, P.R., Feldman, R.G., and Sullivan, M.H.F. (2005). Bacteria and inflammatory cells in fetal membranes do not always cause preterm labor. Pediatr. Res. *57*, 404–411. https://doi.org/10.1203/01.PDR.0000153869.96337.90.

45. Stout, M.J., Conlon, B., Landeau, M., Lee, I., Bower, C., Zhao, Q., Roehl, K.A., Nelson, D.M., Macones, G.A., and Mysorekar, I.U. (2013). Identification of intracellular bacteria in the basal plate of the human placenta in term and preterm gestations. Am. J. Obstet. Gynecol. *208*, 226.e1–226.e7. https://doi.org/10.1016/j.ajog.2013.01.018.

46. Seferovic, M.D., Pace, R.M., Carroll, M., Belfort, B., Major, A.M., Chu, D.M., Racusin, D.A., Castro, E.C., Muldrew, K.L., Versalovic, J., and Aagaard, K.M. (2019). Visualization of microbes by 16S in situ hybridization in term and preterm placentas without intraamniotic infection. Am. J. Obstet. Gynecol. *221*, 146.e1–146.e23. https://doi.org/10.1016/j.ajog.2019.04.036.

47. Seferovic, M., Sánchez-San Martín, C., Tardif, S.D., Rutherford, J., Castro, E.C.C., Li, T., Hodara, V.L., Parodi, L.M., Giavedoni, L., Layne-Colon, D., et al. (2018). Experimental zika virus infection in the pregnant common marmoset induces spontaneous fetal loss and neurodevelopmental abnormalities. Sci. Rep. *8*, 6851. https://doi.org/10.1038/s41598-018-25205-1.

48. Seferovic, M.D., Turley, M., Valentine, G.C., Rac, M., Castro, E.C.C., Major, A.M., Sanchez, B., Eppes, C., Sanz-Cortes, M., Dunn, J., et al. (2019). Clinical importance of placental testing among suspected cases of congenital zika syndrome. Int. J. Mol. Sci. *20*, 712. https://doi.org/10.3390/ijms20030712.

49. Valentine, G.C., Seferovic, M.D., Fowler, S.W., Major, A.M., Gorchakov, R., Berry, R., Swennes, A.G., Murray, K.O., Suter, M.A., and Aagaard, K.M. (2018). Timing of gestational exposure to Zika virus is associated with postnatal growth restriction in a murine model. Am. J. Obstet. Gynecol. *219*. 403.e1-403403.e9. https://doi.org/10.1016/j.ajog.2018.06.005.

50. Rosenberg, A.Z., Yu, W., Hill, D.A., Reyes, C.A., and Schwartz, D.A. (2017). Placental pathology of zika virus: viral infection of the placenta induces villous stromal macrophage (Hofbauer cell) proliferation and hyperplasia. Arch. Pathol. Lab Med. *141*, 43–48. https://doi.org/10.5858/arpa.2016-0401-OA.

51. Cao, B., and Mysorekar, I.U. (2014). Intracellular bacteria in placental basal plate localize to extravillous trophoblasts. Placenta *35*, 139–142. https://doi.org/10.1016/j.placenta.2013.12.007.

52. Fichorova, R.N., Onderdonk, A.B., Yamamoto, H., Delaney, M.L., DuBois, A.M., Allred, E., and Leviton, A.; Extremely Low Gestation Age Newborns ELGAN Study Investigators (2011). Maternal microbe-specific modulation of inflammatory response in extremely low-gestational-age newborns. mBio *2*, e00280-10. https://doi.org/10.1128/mBio.00280-10.

53. Cardenas, I., Means, R.E., Aldo, P., Koga, K., Lang, S.M., Booth, C.J., Manzur, A., Oyarzun, E., Romero, R., Mor, G., and Mor, G. (2010). Viral infection of the placenta leads to fetal inflammation and sensitization to bacterial products predisposing to preterm labor. J. Immunol. *185*, 1248–1257. https://doi.org/10.4049/jimmunol.1000289.

54. Roberts, D.J., Celi, A.C., Riley, L.E., Onderdonk, A.B., Boyd, T.K., Johnson, L.C., and Lieberman, E. (2012). Acute histologic chorioamnionitis at term: nearly always noninfectious. PLoS One *7*, e31819. https://doi.org/10.1371/journal.pone.0031819.

55. Combs, C.A., Gravett, M., Garite, T.J., Hickok, D.E., Lapidus, J., Porreco, R., Rael, J., Grove, T., Morgan, T.K., Clewell, W., et al. (2014). Amniotic fluid infection, inflammation, and colonization in preterm labor with intact membranes. Am. J. Obstet. Gynecol. *210*, 125.e1. https://doi.org/10.1016/j.ajog.2013.11.032.

56. Romero, R., Miranda, J., Chaiworapongsa, T., Chaemsaithong, P., Gotsch, F., Dong, Z., Ahmed, A.I., Yoon, B.H., Hassan, S.S., Kim, C.J., et al. (2015). Sterile intra-amniotic inflammation in asymptomatic patients with a sonographic short cervix: prevalence and clinical significance. J. Matern. Fetal Neonatal Med. *28*, 1343–1359. https://doi.org/10.3109/14767058.2014.954243.

57. Bolte, E., Seferovic, M., Valentine, G.C., Jochum, M., Prince, A., Chu, D., Pace, R., Fowler, S., Swennes, A., Versalovic, J., and Aagaard, K.M. (2020). 695: maternal microbial conventionalization alters type I interferon signaling in mice. Am. J. Obstet. Gynecol. *222*, S439–S440. https://doi.org/10.1016/j.ajog.2019.11.709.

58. Bolte, E.E., Moorshead, D., and Aagaard, K.M. (2022). Maternal and early life exposures and their potential to influence development of the microbiome. Genome Med. *14*, 4. https://doi.org/10.1186/s13073-021-01005-7.

59. Lum, F.M., Narang, V., Hue, S., Chen, J., McGovern, N., Rajarethinam, R., Tan, J.J., Amrun, S.N., Chan, Y.H., Lee, C.Y., et al. (2019). Immunological observations and transcriptomic analysis of trimester-specific full-term placentas from three Zika virus-infected women. Clin. Transl.

Immunology *8*, e01082. https://doi.org/10.1002/cti2.1082.

60. Tsang, J.C.H., Vong, J.S.L., Ji, L., Poon, L.C.Y., Jiang, P., Lui, K.O., Ni, Y.-B., To, K.F., Cheng, Y.K.Y., Chiu, R.W.K., and Lo, Y.M.D. (2017). Integrative single-cell and cell-free plasma RNA transcriptomics elucidates placental cellular dynamics. Proc. Natl. Acad. Sci. USA *114*, E7786–E7795. https://doi.org/10.1073/pnas.1710470114.

61. Pique-Regi, R., Romero, R., Tarca, A.L., Sendler, E.D., Xu, Y., Garcia-Flores, V., Leng, Y., Luca, F., Hassan, S.S., and Gomez-Lopez, N. (2019). Single cell transcriptional signatures of the human placenta in term and preterm parturition. Elife *8*, e52004. https://doi.org/10.7554/elife.52004 PMID - 31829938.

62. Yang, Y., Guo, F., Peng, Y., Chen, R., Zhou, W., Wang, H., OuYang, J., Yu, B., and Xu, Z. (2021). Transcriptomic profiling of human placenta in gestational diabetes mellitus at the single-cell level. Front. Endocrinol. *12*, 679582. https://doi.org/10.3389/fendo.2021.679582.

63. CDC (2022). Variants and genomic surveillance for SARS-CoV-2 in Texas. https://www.dshs.texas.gov/coronavirus/variants-data/.

64. Christensen, P.A., Olsen, R.J., Long, S.W., Subedi, S., Davis, J.J., Hodjat, P., Walley, D.R., Kinskey, J.C., Ojeda Saavedra, M., Pruitt, L., et al. (2022). Delta variants of SARS-CoV-2 cause significantly increased vaccine breakthrough COVID-19 cases in Houston, Texas. Am. J. Pathol. *192*, 320–331. https://doi.org/10.1016/j.ajpath.2021.10.019.

65. Roberts, D.J., Edlow, A.G., Romero, R.J., Coyne, C.B., Ting, D.T., Hornick, J.L., Zaki, S.R., Das Adhikari, U., Serghides, L., Gaw, S.L., et al. (2021). A standardized definition of placental infection by SARS-CoV-2, a consensus statement from the national institutes of health/eunice kennedy shriver national institute of child health and human development SARS-CoV-2 placental infection workshop. Am. J. Obstet. Gynecol. *225*, 593.e1. https://doi.org/10.1016/j.ajog.2021.07.029.

66. Barrozo, E.R., and Aagaard, K.M. (2022). Human placental biology at single-cell resolution: a contemporary review. BJOG *129*, 208–220. https://doi.org/10.1111/1471-0528.16970.

67. Butler, A., Hoffman, P., Smibert, P., Papalexi, E., and Satija, R. (2018). Integrating single-cell transcriptomic data across different conditions, technologies, and species. Nat. Biotechnol. *36*, 411–420. https://doi.org/10.1038/nbt.4096.

68. Chen, E.Y., Tan, C.M., Kou, Y., Duan, Q., Wang, Z., Meirelles, G.V., Clark, N.R., and Ma'ayan, A. (2013). Enrichr: interactive and collaborative HTML5 gene list enrichment analysis tool. BMC Bioinf. *14*, 128. https://doi.org/10.1186/1471-2105-14-128.

69. Huang, R., Grishagin, I., Wang, Y., Zhao, T., Greene, J., Obenauer, J.C., Ngan, D., Nguyen, D.-T., Guha, R., Jadhav, A., et al. (2019). The NCATS BioPlanet – an integrated platform for exploring the universe of cellular signaling pathways for toxicology, Systems

biology, and chemical genomics. Front. Pharmacol. *10*, 445. https://doi.org/10.3389/fphar.2019.00445.

70. Fabregat, A., Jupe, S., Matthews, L., Sidiropoulos, K., Gillespie, M., Garapati, P., Haw, R., Jassal, B., Korninger, F., May, B., et al. (2018). The reactome pathway knowledgebase. Nucleic Acids Res. *46*, D649–D655. https://doi.org/10.1093/nar/gkx1132.

71. Gillespie, M., Jassal, B., Stephan, R., Milacic, M., Rothfels, K., Senff-Ribeiro, A., Griss, J., Sevilla, C., Matthews, L., Gong, C., et al. (2022). The reactome pathway knowledgebase 2022. Nucleic Acids Res. *50*, D687–D692. https://doi.org/10.1093/nar/gkab1028.

72. Takada, K., Shimodai-Yamada, S., Suzuki, M., Trinh, Q.D., Takano, C., Kawakami, K., Asai-Sato, M., Komatsu, A., Okahashi, A., Nagano, N., et al. (2022). Restriction of SARS-CoV-2 replication in the human placenta. Placenta *127*, 73–76. https://doi.org/10.1016/j.placenta.2022.07.010.

73. Trapnell, C., Cacchiarelli, D., Grimsby, J., Pokharel, P., Li, S., Morse, M., Lennon, N.J., Livak, K.J., Mikkelsen, T.S., and Rinn, J.L. (2014). The dynamics and regulators of cell fate decisions are revealed by pseudotemporal ordering of single cells. Nat. Biotechnol. *32*, 381–386. https://doi.org/10.1038/nbt.2859.

74. Cao, J., Spielmann, M., Qiu, X., Huang, X., Ibrahim, D.M., Hill, A.J., Zhang, F., Mundlos, S., Christiansen, L., Steemers, F.J., et al. (2019). The single-cell transcriptional landscape of mammalian organogenesis. Nature *566*, 496–502. https://doi.org/10.1038/s41586-019-0969-x.

75. Abbas, A., Vu Manh, T.P., Valente, M., Collinet, N., Attaf, N., Dong, C., Naciri, K., Chelbi, R., Brelurut, G., Cervera-Marzal, I., et al. (2020). The activation trajectory of plasmacytoid dendritic cells in vivo during a viral infection. Nat. Immunol. *21*, 983–997. https://doi.org/10.1038/s41590-020-0731-4.

76. Bian, Z., Gong, Y., Huang, T., Lee, C.Z.W., Bian, L., Bai, Z., Shi, H., Zeng, Y., Liu, C., He, J., et al. (2020). Deciphering human macrophage development at single-cell resolution. Nature *582*, 571–576. https://doi.org/10.1038/s41586-020-2316-7.

77. Nahrendorf, M., and Swirski, F.K. (2016). Abandoning M1/M2 for a network model of macrophage function. Circ. Res. *119*, 414–417. https://doi.org/10.1161/CIRCRESAHA.116.309194.

78. Aagaard-Tillery, K.M., Silver, R., and Dalton, J. (2006). Immunology of normal pregnancy. Semin. Fetal Neonatal Med. *11*, 279–295. https://doi.org/10.1016/j.siny.2006.04.003.

79. Ivashkiv, L.B. (2013). Epigenetic regulation of macrophage polarization and function. Trends Immunol. *34*, 216–223. https://doi.org/10.1016/j.it.2012.11.001.

80. Murray, P.J. (2017). Macrophage polarization. Annu. Rev. Physiol. *79*, 541–566. https://doi.org/10.1146/annurev-physiol-022516-034339.

81. Yao, Y., Xu, X.H., and Jin, L. (2019). Macrophage polarization in physiological and pathological pregnancy. Front. Immunol. *10*,

792. https://doi.org/10.3389/fimmu.2019.00792.

82. Mues, B., Langer, D., Zwadlo, G., and Sorg, C. (1989). Phenotypic characterization of macrophages in human term placenta. Immunology 67, 303–307.

83. Bulmer, J.N., and Johnson, P.M. (1984). Macrophage populations in the human placenta and amniochorion. Clin. Exp. Immunol. 57, 393–403.

84. Loegl, J., Hiden, U., Nussbaumer, E., Schliefsteiner, C., Cvitic, S., Lang, I., Wadsack, C., Huppertz, B., and Desoye, G. (2016). Hofbauer cells of M2a, M2b and M2c polarization may regulate feto-placental angiogenesis. Reproduction 152, 447–455. https://doi.org/10.1530/REP-16-0159.

85. Schliefsteiner, C., Ibesich, S., and Wadsack, C. (2020). Placental Hofbauer cell polarization resists inflammatory cues in vitro. Int. J. Mol. Sci. 21, 736. https://doi.org/10.3390/ijms21030736.

86. Ben Amara, A., Gorvel, L., Baulan, K., Derain-Court, J., Buffat, C., Vérollet, C., Textoris, J., Ghigo, E., Bretelle, F., Maridonneau-Parini, I., and Mege, J.L. (2013). Placental macrophages are impaired in chorioamnionitis, an infectious pathology of the placenta. J. Immunol. 191, 5501–5514. https://doi.org/10.4049/jimmunol.1300988.

87. Thomas, J.R., Appios, A., Zhao, X., Dutkiewicz, R., Donde, M., Lee, C.Y.C., Naidu, P., Lee, C., Cerveira, J., Liu, B., et al. (2021). Phenotypic and functional characterization of first-trimester human placental macrophages, Hofbauer cells. J. Exp. Med. 218, e20200891. https://doi.org/10.1084/jem.20200891.

88. Constantino, F.B., Cury, S.S., Nogueira, C.R., Carvalho, R.F., and Justulin, L.A. (2021). Prediction of non-canonical routes for SARS-CoV-2 infection in human placenta cells. Front. Mol. Biosci. 8, 614728. https://doi.org/10.3389/fmolb.2021.614728.

89. Zheng, Q.-L., Duan, T., and Jin, L.-P. (2020). Single-cell RNA expression profiling of ACE2 and AXL in the human maternal–Fetal interface. Reprod. Dev. Med. 4, 7–10. https://doi.org/10.4103/2096-2924.278679.

90. Liu, Y., Beyer, A., and Aebersold, R. (2016). On the dependency of cellular protein levels on mRNA abundance. Cell 165, 535–550. https://doi.org/10.1016/j.cell.2016.03.014.

91. Zeng, C., Evans, J.P., King, T., Zheng, Y.M., Oltz, E.M., Whelan, S.P.J., Saif, L.J., Peeples, M.E., and Liu, S.L. (2022). SARS-CoV-2 spreads through cell-to-cell transmission. Proc. Natl. Acad. Sci. USA. 119, e2111400119. https://doi.org/10.1073/pnas.2111400119.

92. Chertow, D., Stein, S., Ramelli, S., Grazioli, A., Chung, J.-Y., Singh, M., Yinda, C.K., Winkler, C., Dickey, J., Ylaya, K., et al. (2021). SARS-CoV-2 infection and persistence throughout the human body and brain. Preprint at Research Square. https://doi.org/10.21203/rs.3.rs-1139035/v1.

93. Van Cleemput, J., van Snippenberg, W., Lambrechts, L., Dendooven, A., D'Onofrio, V., Couck, L., Trypsteen, W., Vanrusselt, J., Theuns, S., Vereecke, N., et al. (2021). Organ-specific genome diversity of replication-competent SARS-CoV-2. Nat. Commun. 12, 6612. https://doi.org/10.1038/s41467-021-26884-7.

94. Hessami, K., Norooznezhad, A.H., Monteiro, S., Barrozo, E.R., Abdolmaleki, A.S., Arian, S.E., Zargarzadeh, N., Shekerdemian, L.S., Aagaard, K.M., and Shamshirsaz, A.A. (2022). COVID-19 pandemic and infant neurodevelopmental impairment: a systematic review and meta-analysis. JAMA Netw. Open 5, e2238941. https://doi.org/10.1001/jamanetworkopen.2022.38941.

95. Edlow, A.G., Castro, V.M., Shook, L.L., Kaimal, A.J., and Perlis, R.H. (2022). Neurodevelopmental outcomes at 1 Year in infants of mothers who tested positive for SARS-CoV-2 during pregnancy. JAMA Netw. Open 5, e2215787. https://doi.org/10.1001/jamanetworkopen.2022.15787.

96. Sutton, D., Fuchs, K., D'Alton, M., and Goffman, D. (2020). Universal screening for SARS-CoV-2 in women admitted for delivery. N. Engl. J. Med. 382, 2163–2164. https://doi.org/10.1056/NEJMc2009316.

97. Tsoutsouki, J., Patel, B., Comninos, A.N., Dhillo, W.S., and Abbara, A. (2022). Kisspeptin in the prediction of pregnancy complications. Front. Endocrinol. 13, 942664. https://doi.org/10.3389/fendo.2022.942664.

98. Rochette, L., Zeller, M., Cottin, Y., and Vergely, C. (2021). GDF15: an emerging modulator of immunity and a strategy in COVID-19 in association with iron metabolism. Trends Endocrinol. Metab. 32, 875–889. https://doi.org/10.1016/j.tem.2021.08.011.

99. Sibiak, R., Jankowski, M., Gutaj, P., Mozdziak, P., Kempisty, B., and Wender-Ożegowska, E. (2020). Placental lactogen as a marker of maternal obesity, diabetes, and fetal growth abnormalities: current knowledge and clinical perspectives. J. Clin. Med. 9, 1142. https://doi.org/10.3390/jcm9041142.

100. Kandel, M., MacDonald, T.M., Walker, S.P., Cluver, C., Bergman, L., Myers, J., Hastie, R., Keenan, E., Hannan, N.J., Cannon, P., et al. (2022). PSG7 and 9 (Pregnancy-Specific beta-1 glycoproteins 7 and 9): novel biomarkers for preeclampsia. J. Am. Heart Assoc. 11, e024536. https://doi.org/10.1161/JAHA.121.024536.

101. Xiong, Y., Liu, Y., Cao, L., Wang, D., Guo, M., Jiang, A., Guo, D., Hu, W., Yang, J., Tang, Z., et al. (2020). Transcriptomic characteristics of bronchoalveolar lavage fluid and peripheral blood mononuclear cells in COVID-19 patients. Emerg. Microbes Infect. 9, 761–770. https://doi.org/10.1080/22221751.2020.1747363.

102. Kesmez Can, F., Özkurt, Z., Öztürk, N., and Sezen, S. (2021). Effect of IL-6, IL-8/CXCL8, IP-10/CXCL 10 levels on the severity in COVID 19 infection. Int. J. Clin. Pract. 75, e14970. https://doi.org/10.1111/ijcp.14970.

103. Lorè, N.I., De Lorenzo, R., Rancoita, P.M.V., Cugnata, F., Agresti, A., Benedetti, F., Bianchi, M.E., Bonini, C., Capobianco, A., Conte, C., et al. (2021). CXCL10 levels at hospital admission predict COVID-19 outcome: hierarchical assessment of 53 putative inflammatory biomarkers in an observational study. Mol. Med. 27, 129. https://doi.org/10.1186/s10020-021-00390-4.

104. Zhang, F., Mears, J.R., Shakib, L., Beynor, J.I., Shanaj, S., Korsunsky, I., Nathan, A., Accelerating Medicines Partnership Rheumatoid Arthritis and Systemic Lupus Erythematosus AMP RA/SLE Consortium, Donlin, L.T., and Raychaudhuri, S. (2021). IFN-γ and TNF-α drive a CXCL10+ CCL2+ macrophage phenotype expanded in severe COVID-19 lungs and inflammatory diseases with tissue inflammation. Genome Med. 13, 64. https://doi.org/10.1186/s13073-021-00881-3.

105. Cross, A.R., de Andrea, C.E., Villalba-Esparza, M., Landecho, M.F., Cerundolo, L., Weeratunga, P., Etherington, R.E., Denney, L., Ogg, G., Ho, L.P., et al. (2023). Spatial transcriptomic characterization of COVID-19 pneumonitis identifies immune circuits related to tissue injury. JCI Insight 8, e157837. https://doi.org/10.1172/jci.insight.157837.

106. Raza, M.T., and Mizan, S. (2022). A systemic study on the vulnerability and fatality of prostate cancer patients towards COVID-19 through analysis of the TMPRSS2, CXCL10 and their co-expressed genes. Genomics Inform. 20, e31. https://doi.org/10.5808/gi.22012.

107. Shue, B., Chiramel, A.I., Cerikan, B., To, T.H., Frölich, S., Pederson, S.M., Kirby, E.N., Eyre, N.S., Bartenschlager, R.F.W., Best, S.M., and Beard, M.R. (2021). Genome-wide CRISPR screen identifies RACK1 as a critical host factor for flavivirus replication. J. Virol. 95, e0059621. https://doi.org/10.1128/JVI.00596-21.

108. Buchrieser, J., Dufloo, J., Hubert, M., Monel, B., Planas, D., Rajah, M.M., Planchais, C., Porrot, F., Guivel-Benhassine, F., Van der Werf, S., et al. (2020). Syncytia formation by SARS-CoV-2-infected cells. EMBO J. 39, e106267. https://doi.org/10.15252/embj.2020106267.

109. Gholami, M., Sakhaee, F., Sotoodehnejadnematalahi, F., Zamani, M.S., Ahmadi, I., Anvari, E., and Fateh, A. (2022). Increased risk of COVID-19 mortality rate in IFITM3 rs6598045 G allele carriers infected by SARS-CoV-2 delta variant. Hum. Genomics 16, 60. https://doi.org/10.1186/s40246-022-00434-8.

110. Xu, F., Wang, G., Zhao, F., Huang, Y., Fan, Z., Mei, S., Xie, Y., Wei, L., Hu, Y., Wang, C., et al. (2022). IFITM3 inhibits SARS-CoV-2 infection and is associated with COVID-19 susceptibility. Viruses 14, 2553. https://doi.org/10.3390/v14112553.

111. Brusa, S., Terracciano, D., Bruzzese, D., Fiorenza, M., Stanziola, L., Pinchera, B., Valente, V., Gentile, I., Cittadini, A., Mormile, I., et al. (2022). Circulating tissue inhibitor of metalloproteinases 1 (TIMP-1) at COVID-19 onset predicts severity status. Front. Med. 9, 1034288. https://doi.org/10.3389/fmed.2022.1034288.

112. Benlarbi, M., Laroche, G., Fink, C., Fu, K., Mulloy, R.P., Phan, A., Ariana, A., Stewart, C.M., Prévost, J., Beaudoin-Bussières, G., et al. (2022). Identification and differential usage of a host metalloproteinase entry pathway by SARS-CoV-2 Delta and Omicron.

iScience *25*, 105316. https://doi.org/10.1016/j.isci.2022.105316.

113. Hermann, C.D., Schoeps, B., Eckfeld, C., Munkhbaatar, E., Kniep, L., Prokopchuk, O., Wirges, N., Steiger, K., Häußler, D., Knolle, P., et al. (2021). TIMP1 expression underlies sex disparity in liver metastasis and survival in pancreatic cancer. J. Exp. Med. *218*, e20210911. https://doi.org/10.1084/jem.20210911.

114. Skórzyńska-Dziduszko, K.E., Kimber-Trojnar, Ż., Patro-Małysza, J., Stenzel-Bembenek, A., Oleszczuk, J., and Leszczyńska-Gorzelak, B. (2018). Heat shock proteins as a potential therapeutic target in the treatment of gestational diabetes mellitus: what we know so far. Int. J. Mol. Sci. *19*, 3205. https://doi.org/10.3390/ijms19103205.

115. Stein, S.R., Ramelli, S.C., Grazioli, A., Chung, J.Y., Singh, M., Yinda, C.K., Winkler, C.W., Sun, J., Dickey, J.M., Ylaya, K., et al. (2022). SARS-CoV-2 infection and persistence in the human body and brain at autopsy. Nature *612*, 758–763. https://doi.org/10.1038/s41586-022-05542-y.

116. Suryawanshi, H., Morozov, P., Straus, A., Sahasrabudhe, N., Max, K.E.A., Garzia, A., Kustagi, M., Tuschl, T., and Williams, Z. (2018). A single-cell survey of the human first-trimester placenta and decidua. Sci. Adv. *4*, eaau4788. https://doi.org/10.1126/sciadv.aau4788 PMID - 30402542.

117. Liu, Y., Fan, X., Wang, R., Lu, X., Dang, Y.-L., Wang, H., Lin, H.-Y., Zhu, C., Ge, H., Cross, J.C., and Wang, H. (2018). Single-cell RNA-seq reveals the diversity of trophoblast subtypes and patterns of differentiation in the human placenta. Cell Res. *28*, 819–832. https://doi.org/10.1038/s41422-018-0066-y.

118. Vento-Tormo, R., Efremova, M., Botting, R.A., Turco, M.Y., Vento-Tormo, M., Meyer, K.B., Park, J.-E., Stephenson, E., Polański, K., Goncalves, A., et al. (2018). Single-cell reconstruction of the early maternal–fetal interface in humans. Nature *563*, 347–353. https://doi.org/10.1038/s41586-018-0698-6.

119. Sun, T., Gonzalez, T.L., Deng, N., DiPentino, R., Clark, E.L., Lee, B., Tang, J., Wang, Y., Stripp, B.R., Yao, C., et al. (2020). Sexually dimorphic crosstalk at the maternal-fetal interface. J. Clin. Endocrinol. Metab. *105*, e4831–e4847. https://doi.org/10.1210/clinem/dgaa503.

120. Han, X., Zhou, Z., Fei, L., Sun, H., Wang, R., Chen, Y., Chen, H., Wang, J., Tang, H., Ge, W., et al. (2020). Construction of a human cell landscape at single-cell level. Nature *581*, 303–309. https://doi.org/10.1038/s41586-020-2157-4.

121. Cao, J., O'Day, D.R., Pliner, H.A., Kingsley, P.D., Deng, M., Daza, R.M., Zager, M.A., Aldinger, K.A., Blecher-Gonen, R., Zhang, F., et al. (2020). A human cell atlas of fetal gene expression. Science *370*, eaba7721. https://doi.org/10.1126/science.aba7721.

122. Saha, B., Ganguly, A., Home, P., Bhattacharya, B., Ray, S., Ghosh, A., Rumi, M.A.K., Marsh, C., French, V.A., Gunewardena, S., and Paul, S. (2020). TEAD4 ensures postimplantation development by promoting trophoblast self-renewal: an implication in early human pregnancy loss. Proc. Natl. Acad. Sci. USA *117*, 17864–17875. https://doi.org/10.1073/pnas.2002449117.

123. Guo, C., Cai, P., Jin, L., Sha, Q., Yu, Q., Zhang, W., Jiang, C., Liu, Q., Zong, D., Li, K., et al. (2021). Single-cell profiling of the human decidual immune microenvironment in patients with recurrent pregnancy loss. Cell Discov. *7*, 1. https://doi.org/10.1038/s41421-020-00236-z PMID - 33390590.

124. Shannon, M.J., Baltayeva, J., Castellana, B., Wächter, J., McNeill, G.L., Yoon, J.S., Treissman, J., Le, H.T., Lavoie, P.M., and Beristain, A.G. (2022). Cell trajectory modeling identifies a primitive trophoblast state defined by BCAM enrichment. Development *149*, dev199840. https://doi.org/10.1242/dev.199840.

125. Liu, Z., Zhai, M., Zhang, Q., Yang, T., Wan, Z., Li, J., Liu, X., Xu, B., Du, L., Chan, R.W.S., et al. (2022). Resolving the gene expression maps of human first-trimester chorionic villi with spatial transcriptome. Front. Cell Dev. Biol. *10*, 1060298. https://doi.org/10.3389/fcell.2022.1060298.

126. Palazzo, A.F., and Lee, E.S. (2015). Non-coding RNA: what is functional and what is junk? Front. Genet. *6*, 2. https://doi.org/10.3389/fgene.2015.00002.

127. Jain, A., and Tuteja, G. (2021). PlacentaCellEnrich: a tool to characterize gene sets using placenta cell-specific gene enrichment analysis. Placenta *103*, 164–171. https://doi.org/10.1016/j.placenta.2020.10.029.

128. Karlsson, M., Zhang, C., Méar, L., Zhong, W., Digre, A., Katona, B., Sjöstedt, E., Butler, L., Odeberg, J., Dusart, P., et al. (2021). A single-cell type transcriptomics map of human tissues. Sci. Adv. *7*, eabh2169. https://doi.org/10.1126/sciadv.abh2169.

STAR★METHODS

KEY RESOURCES TABLE

REAGENT or RESOURCE	SOURCE	IDENTIFIER
Antibodies		
Monoclonal mouse-*anti*-SARS-CoV-2 spike diluted 1:500	GeneTex	GTX632604, RRID:AB_2864418
Polyclonal rabbit-*anti*-SARS-CoV-2 nucleocapsid diluted 1:200	GeneTex	GTX135357, RRID:AB_2868464
Polyclonal goat-*anti*-human-CD163 diluted 1 µg/mL	R&D Systems	AF1607, RRID:AB_354889
Biological samples		
Placenta tissue	Texas Children's Hospital	N/A
Chemicals, peptides, and recombinant proteins		
Protease IV	ACD	322336
TRIzol	ThermoFisher	15596018
TURBO DNase (2 units/uL)	Qiagen	AM1907
Critical commercial assays		
Visium Spatial Gene Expression (version 2, for fresh-frozen tissue)	10x Genomics	1000184
ImmPRESS Polymer detection kit	Vector Labs	MP-7451
ImmPRESS Polymer detection kit goat-*anti*-mouse	Vector Labs	MP-7452
ImmPRESS Polymer detection kit horse-*anti*-goat	Vector Labs	MP-7405
Direct-zol miniprep Plus RNA extraction kit	ZymoResearch	R2072
TaqMan Fast Virus 1-Stem Master Mix	ThermoFisher	4444432
RecoverAll Total Nucleic Acid kit	ThermoFisher	AM1975
Deposited data		
Placenta spatial transcriptomics data	This study	Gene Expression Omnibus (GEO) GEO: GSE222987
Single-cell RNA-sequencing data	Ref. Bolte et al.[60]	European Genome-Phenome Archive accession EGAD00001003705
Single-nuclei RNA-sequencing data	Ref. Lum et al.[62]	GEO accession GEO: GSE173193
Single-cell RNA-sequencing data	Ref. Garcia-Flores et al.; Zielgler et al.; Bolte et al.[19,34,61]	dbGaP accessions phs001886.v1.p1, phs001886.v2.p1, and phs001886.v3
Oligonucleotides		
RNAscope probe for bacterial gene *dapB* as a negative control	ACD	310043
RNAscope probe for housekeeping gene *PPIB* as a positive control	ACD	313901
RNAscope probe for SARS-CoV-2 spike	ACD	848561
SARS-CoV-2 spike TaqMan Primer/Probe set	ThermoFisher/Invitrogen	Vi07918636
SARS-CoV-2 nucleoprotein TaqMan Primer/Probe set	ThermoFisher/Invitrogen	Vi07918637
SARS-CoV-2 ORF1ab TaqMan Primer/Probe set	ThermoFisher/Invitrogen	Vi07921935
AcroMetrix COVID-19 RNA Control	ThermoFisher	954519
Software and algorithms		
rStudio (v4.1.1)	R Foundation	https://www.r-project.org/
SpaceRanger (v1.3.0)	10x Genomics	https://support.10xgenomics.com/spatial-gene-expression/software/pipelines/latest/installation
Seurat (v4.0.3)	Ref. Christensen et al.[67]	https://cran.r-project.org/web/packages/Seurat/index.html
Monocle3 (v1.0.0)	Ref. Fabregat et al.; Gillespie et al.[73,74]	http://cole-trapnell-lab.github.io/monocle3/
Prism (v9.2.0)	GraphPad	https://www.graphpad.com/scientific-software/prism/

RESOURCE AVAILABILITY

Lead contact

Requests for further information, resources, and reagents are directed to, and will be fulfilled by, the lead contact, Kjersti Aagaard (aagardt@bcm.edu).

Materials availability

No new reagents were generated in this study.

Data and code availability

- Spatial transcriptomics data were deposited to Gene Expression Omnibus (GEO: GSE222987) and scripts used for bioinformatics analysis are available at https://github.com/Aagaardlab/placenta-spatial-transcriptomics. Published term human placenta scRNA-seq datasets were downloaded and analyzed independently (European Genome-Phenome Archive accession EGAD00001003705, GEO accession GEO: GSE173193, and dbGaP accessions phs001886.v1.p1, phs001886.v2.p1, and phs001886.v3).
- The Loupe Browser annotations for spatial transcriptomics objects are available for download at Open Science Framework (https://osf.io/mbfuv/?view_only=892cd90b5eb04e42bdbc18e04a102336).
- Any additional information required to reanalyze the data reported in this paper is available from the lead contact upon request.

EXPERIMENTAL MODEL AND STUDY PARTICIPANT DETAILS

Study approval

Acquisition, processing, and storage of human placenta samples were approved by the Baylor College of Medicine Internal Review Board (Peribank: Protocol H-26364 and SARS-CoV-2: Protocol H-47345). All samples were de-identified and analyzed in a blinded fashion. Clinical characteristics are listed in Table S2 and case-matched in Table S1.1. At time of enrollment, subject metadata including age, gestational age at delivery, fetal weight, mode of delivery, parity, race, ethnicity, fetal sex, COVID-19 severity, pneumonia, preeclampsia, preterm birth, days of onset between symptoms and delivery, and offspring SARS-CoV-2 RT-qPCR results were collected. Participants information on sex, age, and race were self-reported. Information on gender and socioeconomic status were not collected.

METHOD DETAILS

Spatial transcriptomics

Human placentae from distinct regions including the chorionic villi, decidua, and chorioamniotic membranes, or cross-sections from the parenchyma, were fresh-frozen in optimal cutting temperature solution (FF-OCT). Blocks were cryosectioned and H&E stained directly on Visium Gene Expression slides (version 2, 10X Genomics, Cat. 1000184) and imaged using a Nikon Eclipse SE Ni microscope using a Nikon DS-Ri1 camera, Nikon Plan Apo objective at 10× magnification (0.45 aperture, 0.91 μm/pixel resolution). Tissues were permeabilized and RNA was subject to spatial transcriptomics library preparation including poly(dT) reverse transcription. Libraries were sequenced on the Illumina NovaSeq S4 platform with 2% PhiX at approximately 50 million reads per sample.

Single-cell and spatial transcriptomics analyses

Reads were demultiplexed and aligned to a custom human (GRCh38) and SARS-CoV-2 reference genome (NC_045512.2) using SpaceRanger (v1.3.0) and custom bash scripts. Downstream analyses were done using the package Seurat (v4.0.3) in

rStudio (v4.1.1). Counts matrices were filtered iteratively to exclude low-quality transcriptomes and clusters defined by quality control metrics (e.g. mitochondrial or hemoglobin gene expression). Spatial transcriptomes were normalized and scaled using a negative binomial model (SCTransform) and the top 3,000 most variable transcripts were used for principal component analysis dimension reduction. Spatial and scRNA-seq datasets were integrated using reciprocal PCA of 3,000 reference transcripts before clustering. The first 30 PCA dimensions were used for K-nearest neighbors' analysis, clustered using a Louvain algorithm with the default resolution parameter (0.6), and visualized by unique manifold approximation and projection (UMAP) in two dimensions. Significantly upregulated transcripts were manually examined with EnrichR,[68] PlacentaCellEnrich,[127] and the Human Protein Atlas,[128] and compare to the prediction scores from the term placenta atlas label transfers, for cell and niche cluster annotations. Pseudotime trajectory analysis was done using Monocle3[73,74] (v1.0.0) with starting points denoted in the text.

RT-qPCR

Placental tissue (50-100mg) from FF-OCT blocks were mechanically disrupted, lysed in TRIzol (ThermoFisher, Cat. 15596018), and RNA was extracted using the Direct-zol miniprep Plus RNA extraction kit (ZymoResearch, Cat. R2072) following the manufacturer's protocol. Formalin-fixed paraffin-embedded (FFPE) placental tissue was cut into 10 μm scrolls and RNA was extracted using the RecoverAll Total Nucleic Acid kit (ThermoFisher, Cat. AM1975) following the manufacturer's protocol. RNA was then DNase treated with TURBO DNase (2 units/uL, Qiagen, Cat. AM1907) and normalized to 700 ng per reaction for the FF-OCT tissue and 100 ng per reaction for the FFPE tissue. The TaqMan Fast Virus 1-Stem Master Mix (ThermoFisher, Cat. 4444432) was used for 1-step RT-qPCR with TaqMan Primer/Probe sets for SARS-CoV-2 spike (AssayID: Vi07918636), nucleoprotein (Vi07918637), or ORF1ab (Vi07921935) transcripts. Serial dilutions of the AcroMetrix COVID-19 RNA Control (ThermoFisher, Cat. 954519) starting with 250 copies were used to generate standard curves to calculate the absolute quantities of each transcript. Data were plotted with GraphPad Prism (v9.2.0).

RNAscope

Fresh-frozen cryosections were fixed in cold 10% formalin and permeabilized with Protease IV (ACD, Cat. 322336) for 20 min before hybridization. We probed for bacterial gene *dapB* as a negative control (ACD, Cat. 310043), housekeeping gene *PPIB* as a positive control (ACD, Cat. 313901), and SARS-CoV-2 spike (ACD, Cat. 848561).

Immunohistochemistry

FF-OCT cryosections and FFPE sections were fixed in pre-chilled 10% formalin for an hour at 4°C and blocked with appropriate blocking serum before staining for 30 min with monoclonal mouse-*anti*-SARS-CoV-2 spike antibody (GeneTex, Cat. GTX632604) diluted 1:500, polyclonal rabbit-*anti*-SARS-CoV-2 nucleocapsid antibody (GeneTex, Cat. GTX135357) diluted 1:200, and polyclonal goat-*anti*-human-CD163 antibody (R&D Systems, Cat. AF1607) diluted to 1 μg/mL. The antigen was then visualized with ImmPRESS Polymer detection kit (Vector Labs, Cat. MP-7451) for goat-*anti*-mouse (Vector Labs, Cat. MP-7452) and horse-*anti*-goat (Vector Labs, Cat. MP-7405) following the manufacturer's instructions. Images were captured under bright-field illumination with a Nikon Eclipse 90i microscope, and the objective magnifications are denoted within the figure legends.

QUANTIFICATION AND STATISTICAL ANALYSIS

Statistics

Subject clinical characteristics were analyzed by unpaired two-way t-tests assuming equal variance (significance $p < 0.05$). Wilcoxon rank-sum test was used to identify significantly differentially expressed transcripts ($q < 0.05$; Log_2(fold-change)>2). The statistics tests were denoted in figure legends, the results section, and the STAR Methods section.